ISSN 0429-8284

Whole Number 237

e-Front runners

FUJI ELECTRIC REVIEW

2

2012 VOL.58

Power Semiconductor contributing in energy and environment region

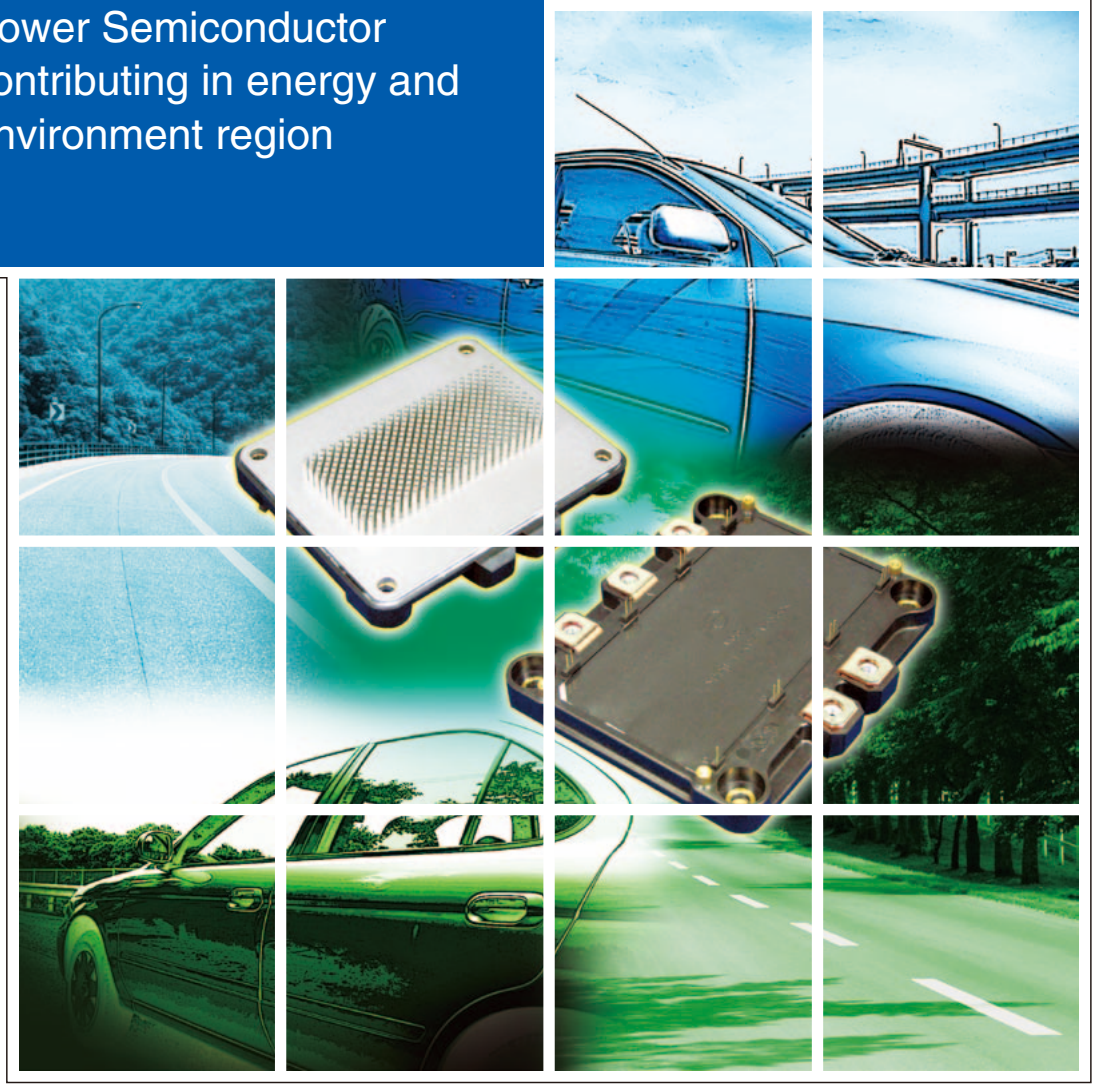

Fuji Electric

e-Front runners

The seeds of energy

The responsibility for protecting the global environment and leaving a secure future for subsequent generations is ours.
Photovoltaic power generation, wind power generation, hybrid cars, electric cars ...
Fuji Electric contributes to the realization of more effective energy utilization and greater energy savings in all fields with high-efficiency, high-precision, and compact and lightweight packages. A creative and abundant future will sprout from these “seeds of energy” Fuji Electric’s power semiconductors.

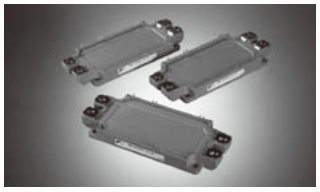
IGBT modules

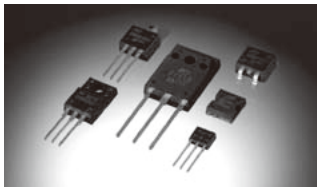
Power MOSFETs

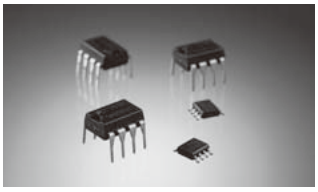
Power ICs

Fuji Electric

FUJI ELECTRIC
REVIEW

2
2012 VOL.58

Power Semiconductor contributing in energy and environment region

CONTENTS

Cover photo:

To help prevent global warming, the popularization of clean energy such as solar power and wind power, as well as the application of power electronics technology that efficiently utilizes this energy, are highly anticipated worldwide.

To response to this heightened anticipation, Fuji Electric has developed various types of power semiconductors having high energy conversion efficiencies and that are environmentally friendly. These devices are utilized in many products in a wide range of fields, including the environment, power generation, automotive, industrial machine, public infrastructure and consumer electronics fields, and are making positive contributions worldwide.

The cover photo is of automotive-use insulated gate bipolar transistor (IGBT) modules that are installed in eco-friendly vehicles such as electric vehicles or hybrid vehicles. Featuring a direct water-cooling structure, these IGBT modules achieve significant reductions in thermal resistance and size in comparison to previous models.

FUJI ELECTRIC REVIEW vol.58 no.2 2012
date of issue: May 20, 2012

editor-in-chief and publisher Naoya Eguchi
Corporate R & D Headquarters
Fuji Electric Co., Ltd.
Gate City Ohsaki, East Tower,
11-2, Osaki 1-chome, Shinagawa-ku,
Tokyo 141-0032, Japan
http://www.fujielectric.co.jp

editorial office Fuji Electric Journal Editorial Office
c/o Fuji Office & Life Service Co., Ltd.
1, Fujimachi, Hino-shi, Tokyo 191-8502, Japan

IGBT Module Series for Advanced-NPC Circuits

Kosuke Komatsu † **Takahito Harada** † **Yoshiyuki Kusunoki** †

ABSTRACT

A series of insulated gate bipolar transistor (IGBT) modules has been developed to enable advanced neutral-point-clamped (A-NPC) inverters. Modules in this series integrate A-NPC circuits for three phases with thermistors in a single package. Loss is minimized by the adoption of 6th-generation IGBT, free wheeling diode (FWD) and reverse blocking IGBT (RB-IGBT) devices. Power dissipation is reduced by 51% compared to conventional two-level inverters and by 33% compared to conventional NPC three-level inverters. Two types of pin configuration are available, and selectable according to customer requirements.

1. Introduction

In recent years, initiatives to reduce CO_2 emissions in order to protect the environment have been implemented in countries throughout the world. The shift to clean energy, such as to wind power and solar power, which does not rely on conventional fossil fuels, is becoming increasingly prominent.

The use of power electronics devices to conserve energy can be found in a wide variety of applications, from consumer electronics to electric railways, FA systems and the like. Moreover, power electronics are used not only in power-consuming applications, but their use has also spread to the fields of power generation, transmission and supply such as in uninterruptible power supplies (UPS), wind power generators and solar power generators. In particular, multi-level inverters have been proposed as an efficient way to increase the power conversion efficiency of a UPS or power generation system[1], and neutral-point-clamped (NPC) inverters have been put into practical use. A 3-level inverter*1 having a simpler circuit configuration than this NPC inverter has also been proposed, but when configured with typical insulated gate bipolar transistor (IGBT) and diode, an increase in conduction loss and a high surge voltage due to the wiring inductance were problems.

Fuji Electric has developed circuit systems for inverters and converters, which are power electronics devices, and has contributed to energy conservation mainly in devices in the industrial field. Additionally, by adopting a custom low inductance package using a reverse-blocking IGBT[2] (RB-IGBT), a proprietarily developed power semiconductor, Fuji Electric has developed an IGBT module for use in advanced NPC (A-NPC) circuits that solves the aforementioned problems[3]. A UPS that utilizes this module has been introduced to the market.

Presently, Fuji Electric is aiming to expand its series of IGBT module for A-NPC circuits, and is developing an IGBT module for A-NPC circuits that integrates a three-phase A-NPC 3-level inverter circuit and a thermistor into a single package. This paper presents an overview of these efforts.

*1: 3-level inverter technology; See supplemental explanation 1 on page 87.

† Fuji Electric Co., Ltd.

2. Characteristics of IGBT Modules for Advanced NPC Circuits

2.1 Overview

An overview of the ratings, dimensions and the like of Fuji Electric's IGBT module series for A-NPC circuits is shown in Table 1. The rated voltage of the main switches is 1,200 V, the rated voltage of the intermediate bidirectional switches is 600 V, and the rated current is 100 A. The modules have the following characteristics.

(a) Integration of a 3-phase A-NPC circuit and a thermistor into a single package
(b) Selectable pin shape according to the inverter production line

Figure 1(a) shows the appearance and Fig. 1(b) shows the equivalent circuit of the IGBT modules.

2.2 Electrical characteristics of the device

(1) Main switches

For the main switches T1 and T2 (see Table 2), the new "V Series" IGBT and free wheeling diode (FWD) having a rated voltage of 1,200 V were used. The V Series has the following characteristics.

Table 1 Overview of IGBT modules for A-NPC circuits

Model	Package dimensions	Rated voltage	Rated current
12MBI100VN-120-50 (Solder pin type)	L122.5×W62.5×H17 (mm)	1,200 V (M10Aain switch part) 600 V (Bidirectional switch part)	100 A (Main switch part) 100 A (Bidirectional switch part)
12MBI100VX-120-50 (Press-fit pin type)			

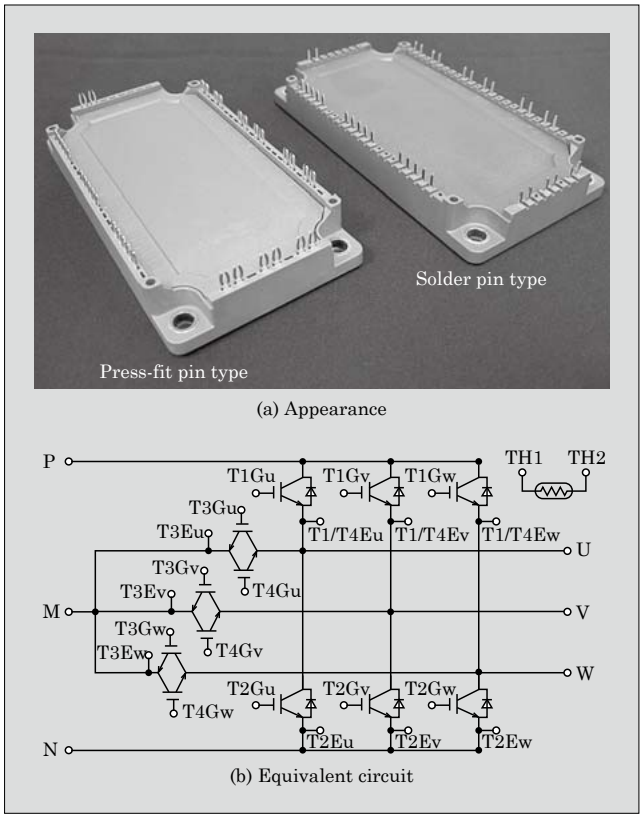

Fig.1 Appearance and equivalent circuit of IGBT module for A-NPC circuits

(a) Lower on-state voltage $V_{CE\ (sat)}$ and less switching loss due to optimized field stop (FS) and trench gate structures

(b) Improved controllability of turn-on di/dt with gate resistance R_g

(2) Bidirectional switches

For the bidirectional switches T3 and T4 (see Table 2), RB-IGBTs having a rated voltage of 600 V were used. The RB-IGBT characteristics are as follows.

(a) RB-IGBT has reverse blocking voltage capability, and can therefore be connected in a anti parallel configuration to enable bidirectional switching.

(b) When a forward gate bias voltage is applied to cause the chip to exhibit reverse recovery switching as a FWD, the reverse recovery characteristics are the same as that of a conventional FWD.

(3) Conduction loss

An A-NPC inverter circuit, as compared to a conventional NPC inverter circuit, has half the number

Table 2 NPC inverter and A-NPC inverter on-state voltage comparison

I_C=100 A, V_{GE}=+15 V, T_j=25 °C

	Current path			
	Mode 1	Mode 2	Mode 3	Mode 4
NPC inverter	3.20 V	3.20 V	3.20 V	3.20 V
A-NPC inverter	1.85 V	1.85 V	2.45 V	2.45 V

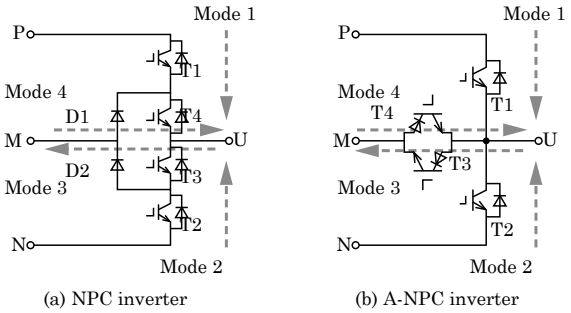

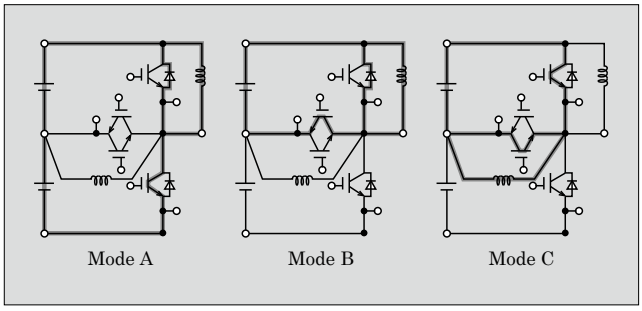

Fig.2 Example of current paths in each switching mode

of conducting elements throughout its entire current path. As a result, conduction loss can be reduced by approximately 30% compared to a conventional NPC inverter. Table 2 compares the current paths and on-state voltages of the conventional NPC inverter and the A-NPC inverter.

(4) Switching loss

An IGBT module for use in A-NPC circuit differs from a conventional IGBT module in that it has the following three switching paths as shown in Fig. 2.

(a) Path in which the main IGBTs operate as switches and the main FWDs operate in reverse recovery (Mode A)

(b) Path in which the RB-IGBTs switch and the main FWDs operate in reverse recovery (Mode B)

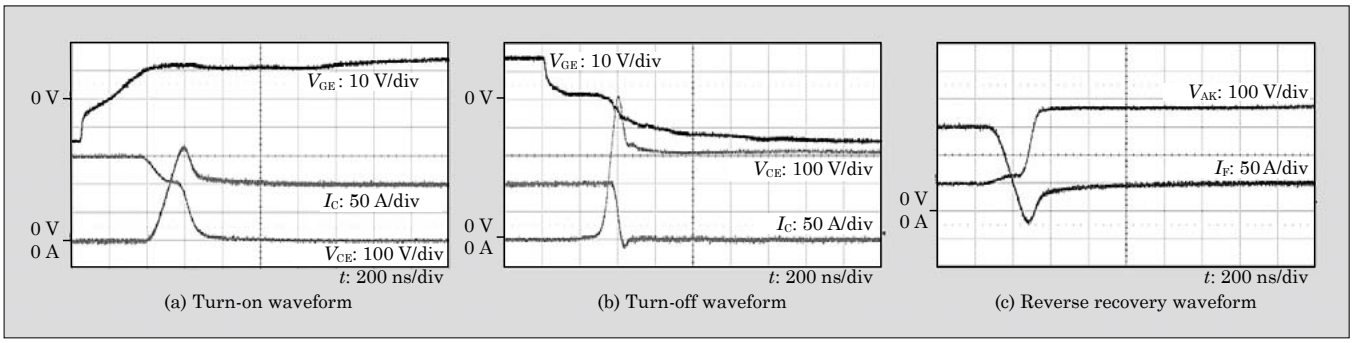

Fig.3 Switching waveform (mode B)

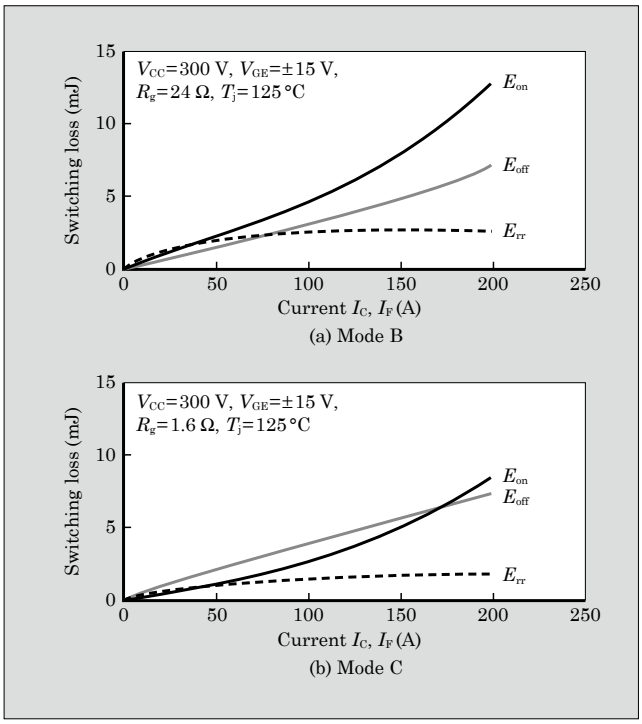

Fig.4 Current dependence of switching loss

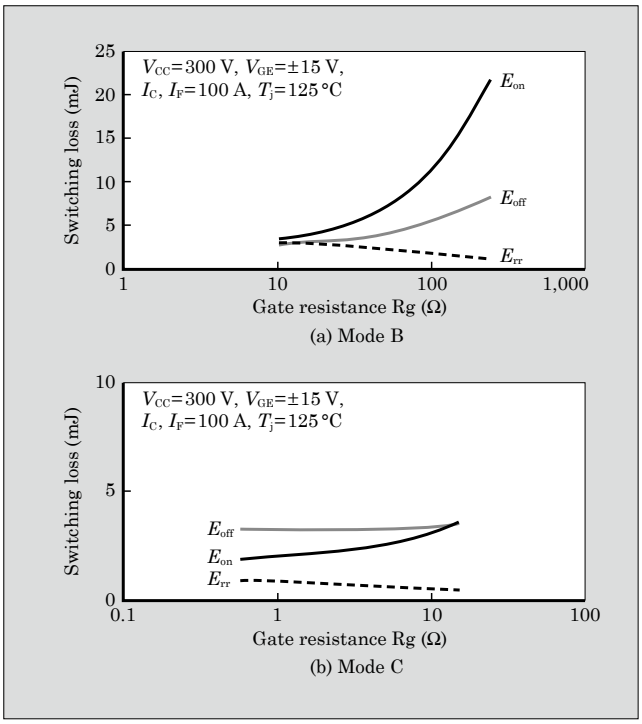

Fig.5 Gate resistance dependence of switching loss

(c) Path in which the main IGBTs switch and the RB-IGBTs operate in reverse recovery (Mode C)

For the 3-level inverter operation, basic operation is in mode B and mode C. Figure 3 shows the turn-on, turn-off and reverse recovery waveforms in mode B for a module at V_{CC}=300 V, I_C=100 A, R_g=24 Ω and T_j=125 °C.

The switching loss is 3.0 mJ at turn-on, 4.1 mJ at turn-off, and 1.67 mJ at reverse recovery, and no turn-off surge that exceeded the rated voltage was found.

Figure 4 shows the current dependence of the switching loss, and Fig. 5 shows the gate resistance dependence of the switching loss. As described above, the reverse-recovery loss characteristics when the RB-IGBT is in reverse-recovery mode C are no different from when a conventional FWD is in reverse-recovery mode B.

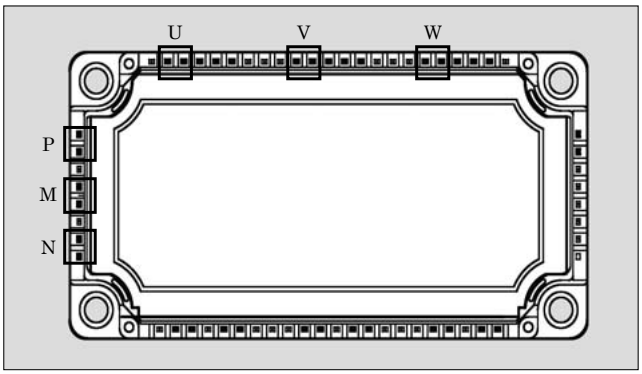

Fig.6 Main terminal arrangement

2.3 Package

A conventional compact package (EconoPIM™*2 3/

*2: EconoPIM™ is a trademark or registered trademark of Infineon Technologies AG.

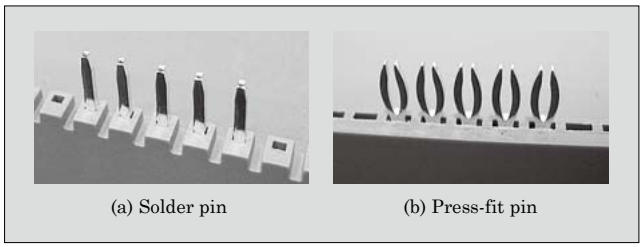

Fig.7 Terminal shape

PC-Pack3) was selected for the newly developed IGBT module for A-NPC circuits. As a result, the package has the following characteristics.

(a) Main terminals P, M, N

Layout allows for easy placement of snubber capacitors (between P-M, between M-N) to reduce surge voltage (see Fig. 6)

(b) Terminal shape

2 types of terminal shapes (solder pin, press-fit pin) can be selected according to customer needs (see Fig. 7)

(c) Environmentally friendly

Lead-free and compliant with RoHS directive*3

3. Power Dissipation

Figure 8 compares the power dissipation per phase of a conventional 2-level inverter, an NPC 3-level inverter and an A-NPC 3-level inverter when operating under the same conditions.

The power dissipation was computed with the V Series ratings of 100 A/1,200 V (EconoPIM™ 3) for the conventional 2-level inverter and using the V Series ratings of 100 A/600 V (EconoPIM™ 3) for the NPC 3-level inverter. Operating conditions for the 20 kVA inverter were f_c=7 kHz, DC voltage=700 V, and output current=30 A (rms). As a result, the A-NPC 3-level inverter exhibited the least power dissipation, 51% less than the conventional 2-level inverter and 33% less than the NPC 3-level inverter. Viewed individually, these inverters have the following characteristics.

The 2-level inverter has the smallest conduction loss since it has only one device that conducts current. However, because the DC voltage is twice that of a 3-level inverter, switching loss accounts for 76.6% of the total power dissipation.

The NPC 3-level inverter has the largest conduction loss since there are two conducting devices in each current flow path. With three levels, however, the DC voltage is halved and the switching loss is less than half that of a 2-level inverter. Consequently, the conduction loss accounts for 54.8% of the power dissipation per phase. As the carrier frequency decreases,

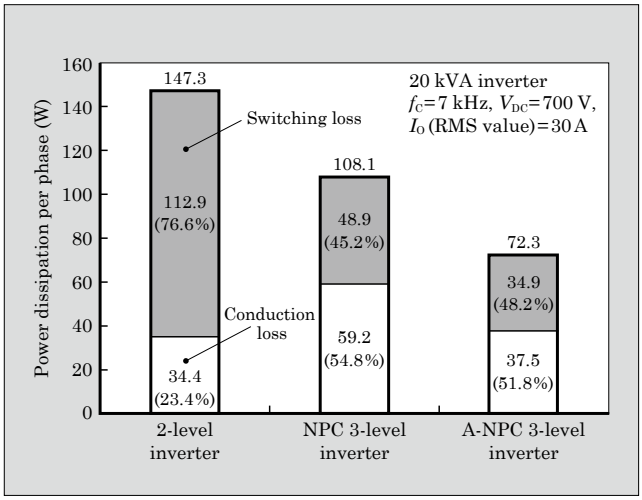

Fig.8 Comparison of power dissipation for various inverters

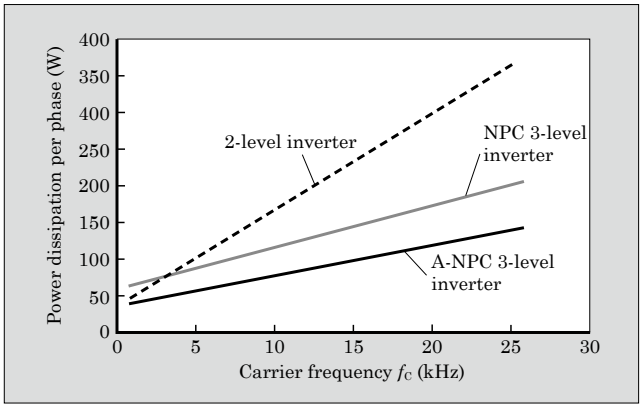

Fig.9 Carrier frequency dependence of power dissipation

conduction loss accounts for a higher percentage of total power dissipation.

With an A-NPC 3-level inverter, because an RB-IGBT has larger conduction loss than an ordinary IGBT, the conduction loss is 8.7% larger than that of a 2-level inverter, but can be reduced to about 37% less than an NPC 3-level inverter. On the other hand, the switching loss is smaller as in the case of the NPC 3-level inverter. As a result, in contrast to the loss in the NPC 3-level inverter, the percentages of conduction loss and switching loss become equal, and even if the carrier frequency changes, the power dissipation never exceeds that of the NPC 3-level inverter.

Figure 9 shows the carrier frequency dependence of power dissipation. In the region of carrier frequencies of 5 kHz or higher, the power dissipation is less for a 3-level inverter than a 2-level inverter. In the region of carrier frequencies lower than 5 kHz, the 2-level inverter appears to have less power dissipation, but the noise filter attached to the inverter apparatus is larger for the 2-level inverter than a 3-level inverter, and as a result, the total loss (power dissipation including fixed loss and filter loss) generated by the entire inverter apparatus, the 3-level inverter has less power dissipation.

*3: RoHS directive: European Union (EU) directive on restriction of the use of certain hazardous substances in electrical and electronic equipment

4. Postscript

This paper has presented an overview and described characteristics of Fuji Electric's IGBT module series for advanced-NPC circuits. This product supports applications of several tens of kVA, and will surely satisfy customer requests for high efficiency, small size and ease of use.

In the future, Fuji Electric will expand the product lineup of this IGBT module series for advanced-NPC circuits, and intends to develop modules in response to requests for higher efficiency in UPSs and the like.

References

(1) Nabae, A. et al. "A New Neutral-Point-Clamped PWM Inverter," IEEE Trans. on I. A., 1981, vol.IA-17, no.5, p.518-523.

(2) Takei, M. et al. "The Reverse Blocking IGBT for Matrix Converter with Ultra-Thin Wafer Technology," Proc. of ISPSD '03, 2003, p.156-159.

(3) Komatsu, K. et al. "New IGBT Modules for Advanced Neutral-Point-Clamped 3-Level Power Converters," Proc. of IPEC '10, 2010, p.523-527.

Direct Liquid Cooling IGBT Module for Automotive Applications

Takahisa Hitachi † **Hiromichi Gohara** † **Fumio Nagaune** †

ABSTRACT

A compact insulated gate bipolar transistor (IGBT) module with low thermal resistance and direct liquid cooling, system has been developed to contribute to reducing the size of user systems. Thermal fluid simulations were used to optimize the liquid cooling fin shape. Square pin fins were selected because of their overall outstanding performance, including heat dissipation performance, cooling liquid flow velocity, and pressure loss. Under optimized liquid flow conditions, measured values of chip temperature were within 2% of simulation values, confirming the accuracy of the simulations. From these results, this IGBT module for direct liquid cooling realizes a 30% reduction in thermal resistance and allow a 40% reduction in size compared to the conventional configuration.

1. Introduction

Hybrid electric vehicles (HEVs), currently the most prevalent type of fuel-efficient cars, have the dual power sources of a internal combustion engine and an electric motor. During acceleration, the motor assists the engine, while during deceleration, regenerative braking acts to charge the battery to improve the fuel efficiency. Because a gasoline engine is used, HEVs can be operated without reliance on quick charger or other infrastructure, and their further popularization in the future is anticipated.

This paper introduces an automotive insulated gate bipolar transistor (IGBT) module suitable for use in drive system inverters in HEVs and electric vehicles (EVs). In order to meet many diverse needs, Fuji Electric plans to create a series of products having specific output power classes, suitable for motor output ratings of up to about 100 kW, and to contribute to the development of fuel-efficient systems for customers such as automobile manufacturers and electric equipment manufacturers.

2. Background

Types of hybrid systems include a 2-motor type equipped with both a drive motor and a generator motor, and a 1-motor type that assists the engine and performs regenerative braking. The 2-motor type is installed mainly in mid-size or large passenger cars and results in a relatively large improvement in fuel efficiency. The 1-motor type is installed mainly in compact cars and although a dramatic improvement in fuel efficiency is not expected, is a small lightweight and relatively low-cost system. In a 2-motor type hybrid system, motors having a relatively large output of 50 kW or greater are used, while for the 1-motor type, motors with output power of 20 kW or less are often used.

Electric vehicles have a battery and a motor as their power source, and do not generate harmful exhaust gas since they do not use fossil fuels when being driven. Additionally, because they have a high well-to-wheel efficiency (efficiency from the primary energy source to actual driving of the vehicle), electric vehicles exhibit a large energy-saving effect and are thought to be the ultimate fuel-efficient car. Motors installed in electric vehicles range from 50 kW to 100 kW according to the body size. A significant reduction in the cost of their batteries, however, is needed in order for electric vehicles to achieve wide-spread adoption. In the meantime, plug-in hybrid electric vehicles (PHEVs) that have been developed to realize higher fuel efficiency performance are being commercialized. Batteries can be charged from household AC power sockets, and through using electric vehicles for short-distance travel and hybrid vehicles that combine an electric motor with engine output for long-distance travel, a dramatic reduction in CO_2 emissions and an increase in cruising distance are anticipated.

In this way, many types of systems are equipped with a motor to save energy, and their output capacities vary from small to large. Accordingly, IGBT modules of various current capacities and voltage classes are used in the inverters in these systems.

A hybrid system is configured from such components as a power control unit (PCU) that controls the power converting function, a motor, a battery and so on. Inside the PCU, IGBTs play a major role in acting as the main switch of an inverter that outputs three-phase alternating current.

Many varieties of IGBT modules have been devel-

† Fuji Electric Co., Ltd.

oped for industrial and consumer applications, and their product lineup is also diverse in terms of current capacity. Because the specifications concerning durability of these IGBT modules were not entirely suitable for automotive applications, however, they could not be used as-is, and instead, custom products were often developed and installed. In the future, as electric drive technology becomes indispensible for reducing fuel consumption and various customer requirements for IGBT modules are received, their use is expected to increase further.

3. Product Concept and Specifications

3.1 Product concept

While meeting diverse customer requirements, We have also considered products that incorporate ideas of its own. With the goal of "contributing to miniaturization of the customer's system," Fuji Electric has significantly improved the heat dissipation performance of IGBT modules while maintaining the required basic performance in order to enhance the power density.

To reduce the size of the module, a direct liquid-cooling structure was adopted and thermal fluid simulations were carried out in order to optimize the fin shape and the liquid flow. A 30% reduction in thermal resistance, compared to a module with a conventional structure, was confirmed. Additionally, reducing the active area of the power chip (die shrink) was also studied. As a result, We determined that a module size 40% smaller than that of a module with a conventional structure could be realized, and began product development. Use of the latest version "V-series" chip, which has already begun to be mass-produced for industrial applications, as the power chip provides an even greater effect.[1]

Next, the design of a module that conforms to the usage conditions (battery voltage: 300 V, max. current (RMS value): 200 A, carrier frequency: 10 kHz) actually requested by customers was examined, and the results of evaluation of prototypes will be described below.

3.2 Product specification

Figure 1 shows the appearance of the IGBT module and Fig. 2 shows its equivalent circuit diagram.

This product is characterized by low thermal resistance as a result of a direct liquid cooling structure, and the high current density has enabled the package size to be reduced significantly. The module has external dimensions of 105×108 (mm), which is approximately 40% smaller than our previous comparable product having a conventional structure. Figure 3 compares cross-sections of the conventional structure and the liquid cooling structure, and Fig. 4 compares their thermal resistances.

In the conventional structure, thermal grease is used to reduce the contact thermal resistance between a copper base and the cooling fin surface. Thermal grease has a large thermal resistance even at thick-

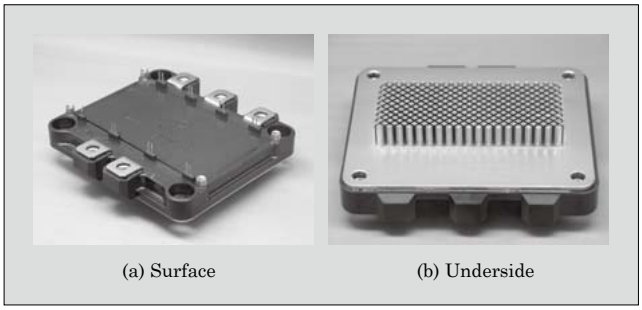

Fig.1 Appearance of M651 (650 V/400 A) module

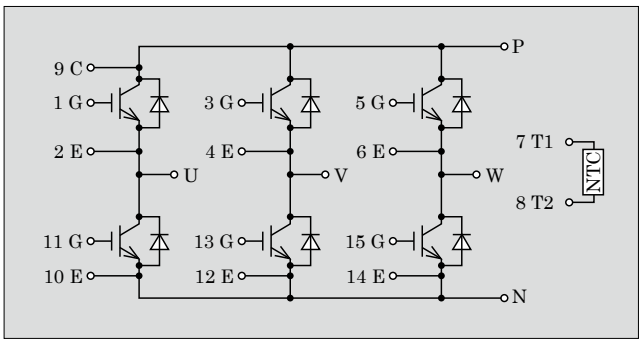

Fig.2 Equivalent circuit of the module

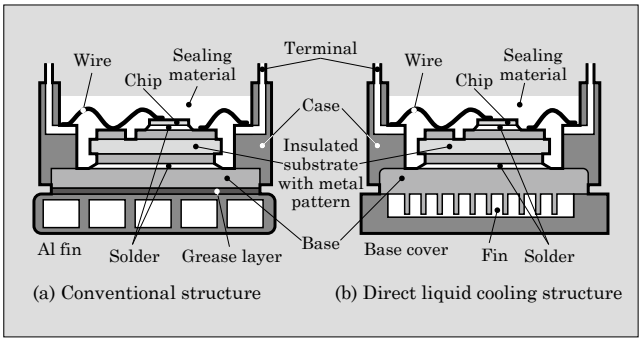

Fig.3 Cross-sectional comparison of conventional structure and direct liquid cooling structure

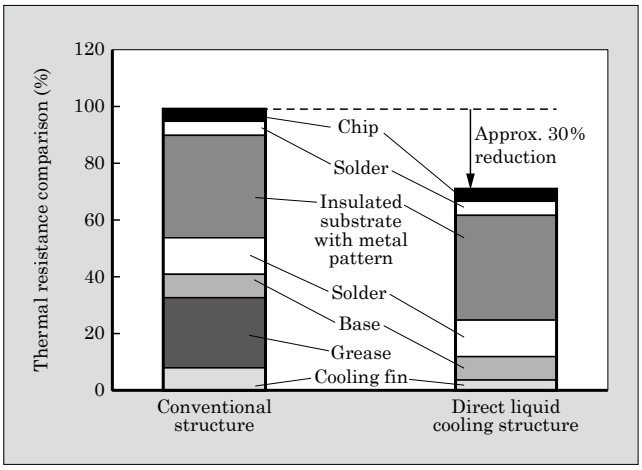

Fig.4 Thermal resistance comparison of conventional structure and direct liquid cooling structure

nesses of several tens of μm, and was unable to conduct waste heat efficiently from the module to the cooling fins. Additionally, an adequate cooling effect could not be obtained since the fluid flow path of the cooling fins did not match the distribution of heat generated by the mounted device. With the newly developed direct liquid cooling structure, the cooling effect was improved by integrating the copper base and the cooling fins so as to eliminate the thermal grease layer. Moreover, by arranging the fins in a high density configuration directly beneath the power chip, which is a heat-generating body, the capacity for heat dissipation between the fins and the cooling liquid is increased. The result is that the thermal resistance between the power chip and the cooling liquid was reduced by approximately 30% compared to that of the conventional structure. By improving the cooling efficiency, the device can be made with higher current density so that more current can flow through a single chip (see Fig.5).

4. Direct Liquid Cooling Technology

4.1 Investigation of heat dissipation performance

With the direct liquid cooling structure, the heat dissipation performance changes according to such factors as the fin shape and the flow direction of the cooling liquid. Fluid simulations were performed for various fin shapes and flow paths in order to optimize the cooling system, and details are presented below.(2)

The IGBT module in an inverter system fulfills the function together with connected smoothing capacitor, circuit board, harness, current sensor and the like. So as to accommodate different system designs from many customers, the fin shape was selected to be a pin-type fin through which cooling fluid could flow in either the width or depth direction. (see Fig.6) Selection of the pin fin cross-sectional shape necessitated a comprehensive examination of the heat dissipating performance, cooling liquid flow velocity and pressure loss, and Fuji Electric investigated the cross-sections of typical round and square pin fins.

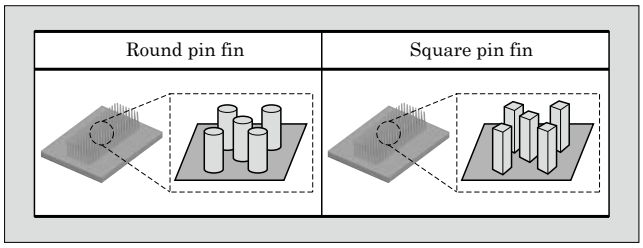

Fig.5 Cooling fin shape

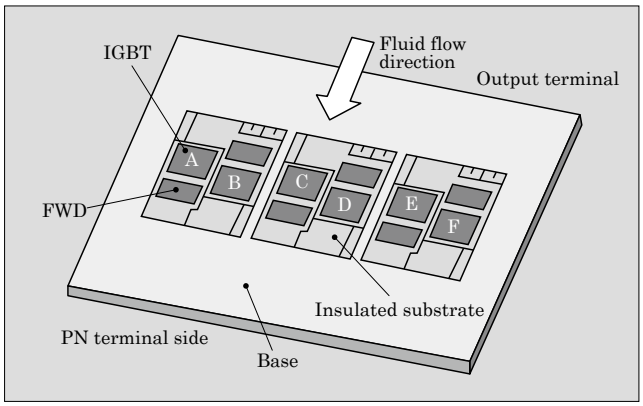

Fig.6 Thermal fluid simulator model

4.2 Optimization of flow path

The flow path was investigated using a thermal fluid simulator (Icepak*1), and the junction temperature, flow velocity of the cooling liquid and pressure loss were computed and compared. Class 2 antifreeze coolant (LLC) 50% is used as the cooling liquid, and the model of the IGBT module shown in Fig. 6 is used as the analysis model. The fins are formed on the underside of the insulated substrate where the heat-generating chip is located. One IGBT chip and one FWD chip are provided in each arm. A single output phase (half bridge) is provided on each insulated substrate. In consideration of the inverter system commonly used and so that the cooling liquid will flow evenly to the fin area, the depth direction shown in Fig. 6 was selected as the direction of fluid flow. Figure 7 shows the structure of a cooling liquid jacket that compares the flow velocities of the cooling liquid.

With the fluid flow direction shown in Fig. 6, the flow of cooling liquid in the fin area becomes nearly constant and uniform. A flow velocity distribution that is uniform, from the liquid inlet to below the insulated substrate, is obtained for each phase, and the cooling performance in each phase is predicted to be equal. Moreover, in order to reduce the pressure loss, because

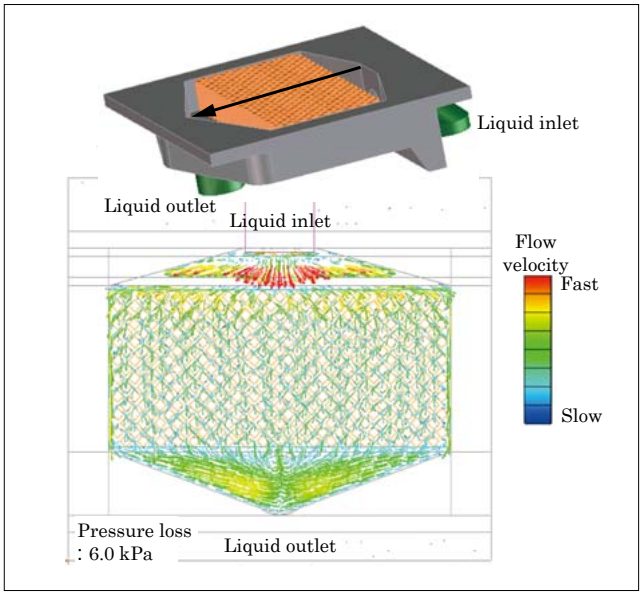

Fig.7 Fluid flow velocity distribution in cooling liquid jacket

*1: Icepak is a trademark or registered trademark of US-based ANSYS, Inc. and its subsidiaries.

the cooling liquid traverses a short distance in passing through the fin area, and the flow velocity of the cooling liquid must be constant in the fin area, the flow path of Fig. 7 is found to enable efficient cooling.

4.3 Selection of the fin shape

Using the cooling liquid jacket of Fig. 7, thermal fluid simulations were performed to select the fin shape in consideration of its effect on junction temperature and pressure loss. The analysis conditions assumed loss at the time of inverter operation, heat generation of 258 W by the IGBT and 31 W by the FWD, a cooling liquid of LLC 50%, a cooling liquid flow rate of 10 L/min, and a cooling liquid temperature of 65 °C.

Figure 8 shows the simulation results of the rise in junction temperature. The junction temperature was verified and compared for each fin shape. The maximum junction temperature was 141.6 °C for round pin fins and 136.0 °C for square pin fins, while the pressure loss was 4.8 kPa for round pin fins and 6.0 kPa for square pin fins. Figure 9 compares the IGBT junction temperature and pressure loss for round pin fins and square pin fins. The round pin fins have a smaller fin volume density, and therefore the pressure loss is less. On the other hand, because the square pin fins have a larger surface area, the junction temperature decreases, but the fin volume density increases and the pressure loss becomes greater. The difference in pressure loss was determined to be about 1 kPa, which is not considered to be a significant difference, and therefore square pin fins were selected so as to fully utilize the cooling performance of direct liquid cooling.

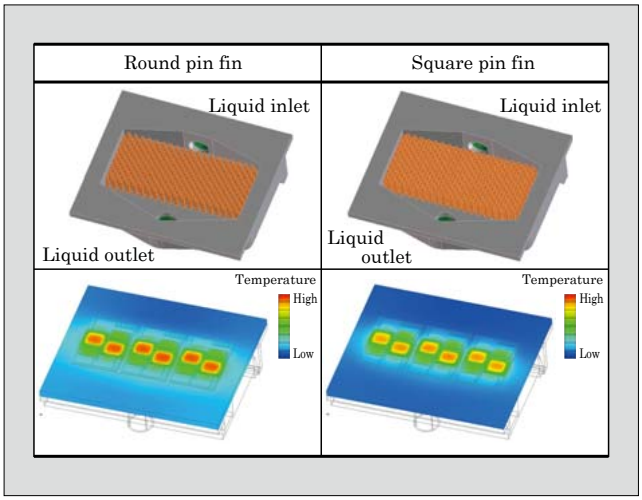

Fig.8 Simulation results of junction temperature rise

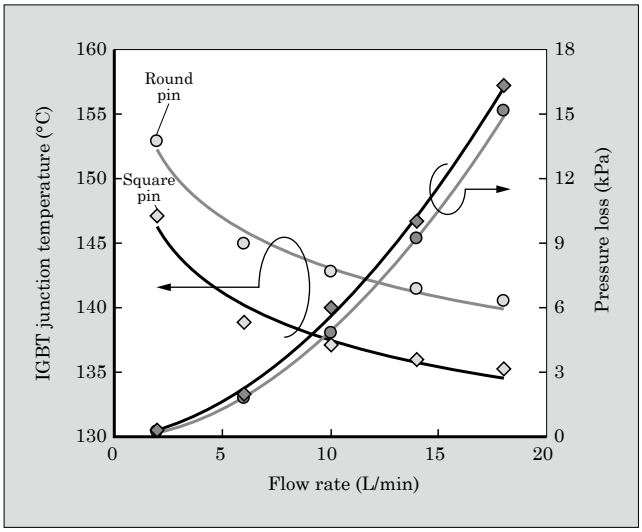

Fig.9 Flow rate dependence of round pin fin and square pin fin IGBT junction temperature and pressure loss (simulation)

4.4 Actual measurement results of junction heat generation

To confirm the validity of the simulation of the cooling performance, the rise in junction temperature of an actual sample was verified. So that the measurement conditions matched those of the simulation, the following conditions were used.

- ○ Loss: IGBT 258 W, FWD 31 W
- ○ Cooling liquid: LLC 50%
- ○ Flow rate: 5 to 15 L/min
- ○ Cooling liquid temperature: 65 °C

In consideration of the aforementioned results, the water jacket used for the measurements was fabricated based on the model of Fig. 7. (see Fig. 10)

A comparison of the square pin fin simulation and measurement results in the case of a flow rate of 10 L/min is shown in Table 1. Columns A through F in Table 1 show the junction temperatures of each

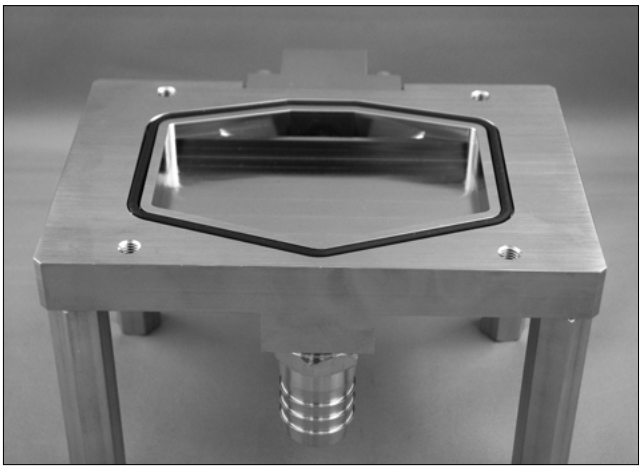

Fig.10 Prototype of cooling liquid jacket

Table 1 Comparison of junction heat generation by simulation and actual measurement (IGBT)

(Units: °C)

	A	B	C	D	E	F
Actual measurement	133.6	137.6	138.4	139.1	136.6	137.7
Simulation	136.7	137.4	137.1	137.6	136.9	136.9
Difference	2.3%	0.1%	0.9%	1.1%	0.2%	0.6%

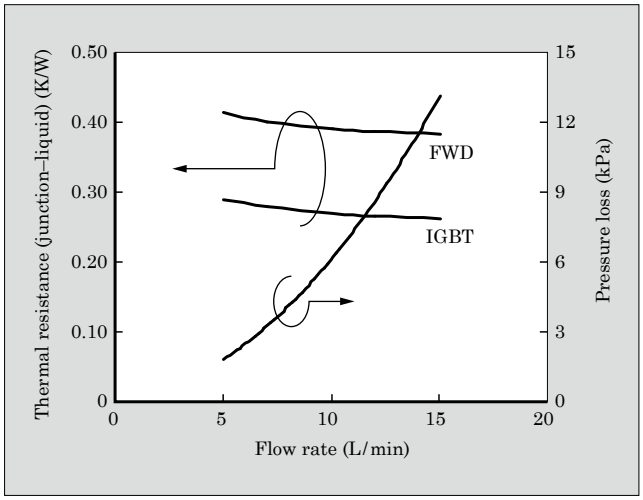

Fig.11 Flow rate dependence of thermal resistance and pressure loss (actual measured values)

chip in Fig. 6. The difference for each phase is at most about 2%, which confirms the equivalence of the simulation and the measurement results. From the measured results, the thermal resistance was calculated to be 0.27 K/W (IGBT average value). While taking the measurements, the flow rate was varied in order to confirm the flow rate dependence of thermal resistance. Figure 11 shows the flow rate dependence (actual measured values) of thermal resistance and pressure loss for flow rates of 5 to 15 L/min.

Comparing the 5 L/min and 15 L/min flow rates, it can be seen that the IGBT and the FWD both exhibited a decrease in thermal resistance by about 10% at 15 L/min, and that by increasing the flow rate, the heat dissipation performance was found to improve. Increasing the flow rate, however, results in a greater loss of pressure, and therefore optimization of the pump performance during use and of the flow path design are needed.

5. Postscript

A direct liquid cooling-type IGBT module for automotive applications has been introduced. The 400 A rated product introduced in this paper will serve as a stepping stone for Fuji Electric's planned development of high-current rated 600 A and 900 A products in the future. We intends to develop a series of products that are widely applicable to inverter systems for motor outputs up to about 100 kW.

We will continue to develop highly reliable, high-performance modules that facilitate system design for an increasing number of users, and to reduce the environmental impact of automobiles.

References

(1) Nakano, H. et al. 600 V trench-gate IGBT with Micro-P structure (Proceedings of the 21th International Symposium on Power Semiconductor Devices and ICs). 2009, p.132-135.
(2) Nagaune, F. et al. Small Size and High Thermal Conductivity IGBT Module for Automotive Applications. PCIM Europe 2011, p.785-790.

Expanded Lineup of High-Power 6th Generation IGBT Module Families

Takuya Yamamoto † **Shinichi Yoshiwatari** † **Hiroaki Ichikawa** †

ABSTRACT

To respond to growing demand in the renewable energy sector, including wind and solar power, Fuji Electric has expanded the lineup of modules in its high-power insulated gate bipolar transistor (IGBT) module families. These new high-power modules feature 6th-generation "V-Series" IGBTs. Operation is guaranteed at maximum junction temperatures up to 175 °C, and the modules deliver industry leading low on-voltage and low switching loss. Reliability is higher than conventional products due to the application of the latest packaging technology, including ultrasonic welded terminals and highly reliable lead-free solder.

1. Introduction

Insulated gate bipolar transistor (IGBT) modules are used widely due to their advantages of low loss, high breakdown resistance, ease of drive circuit design and so on. In the field of high-voltage and high-power device applications, the heretofore widely-used gate turn-off (GTO) thyristors are being replaced with IGBT modules, and IGBT modules are being applied widely to high-power inverters and high voltage inverter units.

In recent years, for the prevention of global warming, the market for renewable energy (wind power generation, solar power generation) has been growing rapidly. In this field, power conversion equipment has progressed to higher capacities, and in particular, the need for high-power IGBT modules has increased greatly. For applications in this field, Fuji Electric has previously developed the high power module (HPM) and PrimePACK™ *1 product series.[1][2]

Recently, in response to diverse customer needs, Fuji Electric has expanded the HPM and PrimePACK™ product series. Equipped with Fuji Electric's 6th generation "V-Series" IGBTs[3], these products achieve the industry's leading level of low on-voltage and, at the same time, low switching loss. Additionally, the latest package technology is applied to realize high power density and high reliability.

This paper presents an overview and describes the characteristics of Fuji Electric's "V-Series HPM Family" of high-power 6th generation IGBT modules.

*1: PrimePACK™ is a trademark or registered trademark of Infineon Technologies AG.

† Fuji Electric Co., Ltd.

2. Product Lineup

Figure 1 shows the appearance of the V-Series HPM Family packages. The PrimePACK™ product series consists of 2-in-1 and chopper module circuit

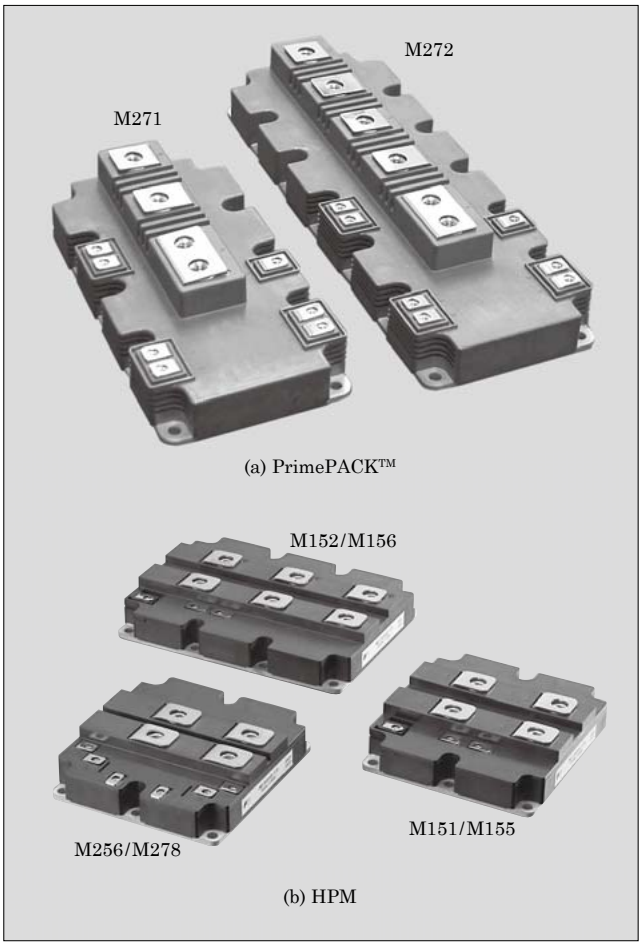

Fig.1 Appearance of V-Series HPM Family packages

Table 1 V-Series HPM Family product lineup

	Product lineup	Product type	Rated voltage (V)	Rated current (A)	Circuit configuration	Package type	Package size (mm)	Insulating substrate	Base material Base thickness
PrimePACK™	E-type	2MBI600VXA-120E-50	1,200	600	2-in-1	M271	172×89×38	Al_2O_3	Copper 3 mm
		2MBI900VXA-120E-50		900					
	P-type	2MBI900VXA-120P-50							
		2MBI1400VXB-120P-50		1,400		M272	250×89×38		
	E-type	2MBI650VXA-170E-50	1,700	650		M271	172×89×38		
		2MBI1000VXB-170E-50		1,000		M272	250×89×38		
		2MBI1000VXB-170EA-50							
		2MBI1400VXB-170E-50		1,400					
	P-type	2MBI1400 VXB-170P-50							
	E-type	1MBI650VXA-170EH-50		650	Chopper	M271	172×89×38		
		1MBI650VXA-170EL-50							
		1MBI1000VXB-170EH-50		1,000		M272	250×89×38		
		1MBI1000VXB-170EL-50							
Industrial-use HPM	TBD*1	1MBI1200VC-120*1	1,200	1,200	1-in-1	M151	130×140×38	Si_3N_4	Copper 5 mm
		1MBI1600VC-120*1		1,600					
		1MBI2400VC-120*1		2,400					
		1MBI2400VD-120*1		2,400		M152	190×140×38		
		1MBI3600VD-120*1		3,600					
		2MBI600VG-120*1		600	2-in-1	M256	130×140×38		
		2MBI800VG-120*1		800					
		2MBI1200VG-120*1		1,200					
	E-type	1MBI1200VC-170E	1,700	1,200	1-in-1	M151	130×140×38		
		1MBI1600VC-170E		1,600					
		1MBI2400VC-170E		2,400					
		1MBI2400VD-170E		2,400		M152	190×140×38		
		1MBI3600VD-170E		3,600					
		2MBI600VG-170E		600	2-in-1	M256	130×140×38		
		2MBI800VG-170E		800					
		2MBI1200VG-170E		1,200					
Traction-use HPE		1MBI1200VR-170E*2		1,200	1-in-1	M155	130×140×38	AlN	Al SiC
		1MBI1600VR-170E*2		1,600					
		1MBI2400VR-170E*2		2,400					
		1MBI2400VS-170E*2		2,400		M156	190×140×38		
		1MBI3600VS-170E*2		3,600					
		2MBI600VT-170E*2		600	2-in-1	M278	130×140×38		
		2MBI800VT-170E*2		800					
		2MBI1200VT-170E*2		1,200					

*1 : TBD : To Be Determined
*2 : underdevelopment

configurations, 1,200 V and 1,700 V class ratings, and current capacities of 600 to 1,400 A. The HPM product series consists of 1-in-1 and 2-in-1 module circuit configurations, 1,200 V and 1,700 V class ratings, and current capacities of 600 to 3,600 A. Table 1 lists the lineup of the V-Series HPM Family product series.

3. Electrical Characteristics

Incorporating a V-Series IGBT, the V-Series HPM Family of products guarantees non-continuous operation up to a maximum chip junction temperature of T_{jmax}=175 °C for momentary abnormal states, and guarantees normal operation at an operating temperature of T_{jop}=150 °C. By improving reliability and breakdown resistance during high-temperature operation, each of these temperatures was increased by 25 °C compared to those of the 5th generation "U-Series" IGBT modules.

3.1 IGBT chip characteristics

Because a high-power IGBT module will instantaneously cut off a large current, the surge voltage generated at turn-off is large. For the V-Series HPM

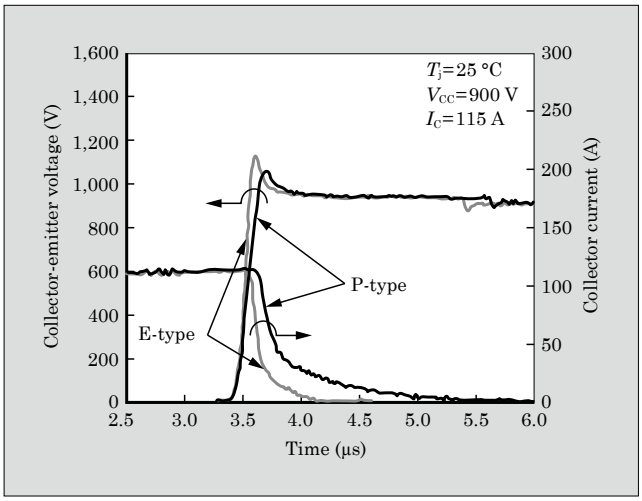

Fig.2 Comparison of IGBT turn-off switching waveforms

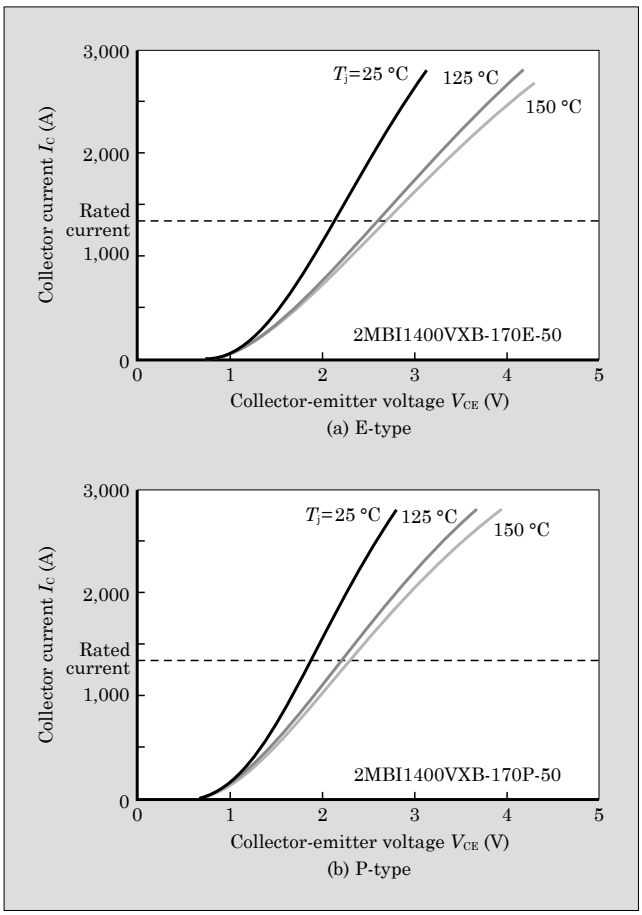

Fig.3 $V_{CE(sat)}$-I_C characteristics

Family, in addition to the previous (E-type) lineup of V-Series IGBT chips, an IGBT chip product lineup (P-type) having soft switching characteristics was newly developed by adjusting the IGBT chip characteristics for applications in the high-power device field. Figure 2 shows a comparison of the switching waveforms at turn-off for E-type and P-type 1,700 V-IGBT chips. Compared to the E-type, the P-type has a slower di/dt at turn-off, and achieves a lower turn-off surge

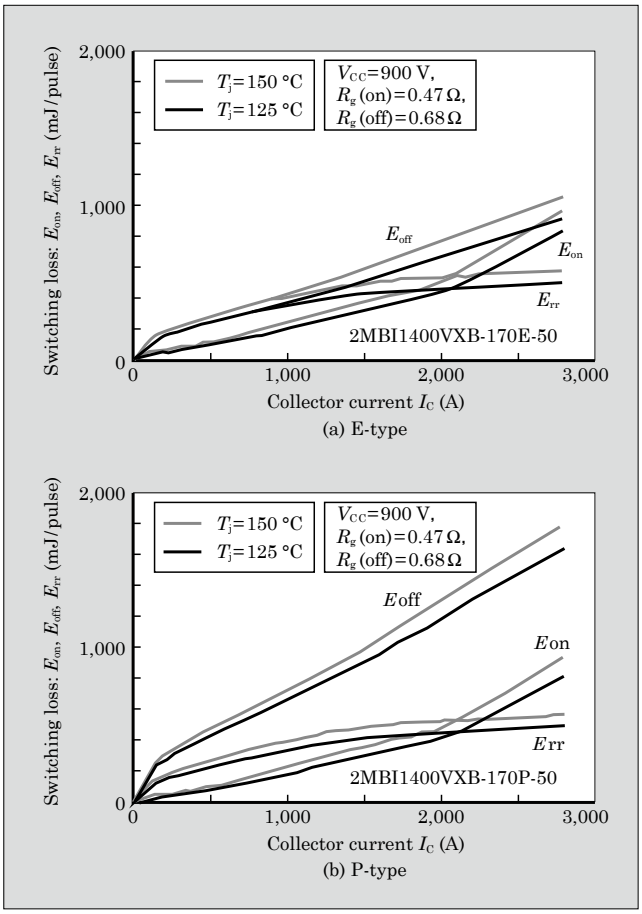

Fig.4 Switching loss vs. current characteristic

voltage. Electrical characteristics are described below for the example of a 1,700 V/1,400 A module.

3.2 V-I characteristics

Figure 3 shows I_C vs. $V_{CE(sat)}$ characteristics of the module. Comparing the E-type and the P-type reveals that at the rated current of I_C=1,400 A and T_j=125 °C, the characteristic of the P-type is about 0.4 V lower.

3.3 Switching characteristics

Figure 4 shows the switching loss vs. current characteristic. In terms of turn-on loss and reverse recovery loss, the E-type and the P-type are the same, but the turn-off loss is about 1.8 times larger for the P-type.

As described above, the V-Series HPM Family contains two types of product lines with different IGBT chip characteristics so that suitable products can be provided for the drive conditions of our customers.

4. Package Structure

Power conversion equipment in the renewable energy field and elsewhere must have high reliability in order to provide a stable supply of electric power.[4] The V-Series HPM Family uses the latest package technology to ensure long-term reliability.

Figure 5 shows a cross-sectional schematic view of an IGBT module. Connecting a conducting/blocking electrical load to an IGBT module causes thermal stress is generated in the junction of the IGBT. The use of materials having a low coefficient difference of thermal expansion in the junction ensures high thermal cycling capability. Table 2 lists the technologies and materials applied to the V-Series HPM Family. The PrimePACK™ series uses ultrasonic welding technology and highly reliable lead-free solder material to achieve higher reliability than in previous products. The HPM product line uses a 5 mm-thick base, or an AlSiC base for traction applications, to achieve even longer term reliability.

4.1 Application of ultrasonic terminal welding technology

Figure 6 shows the external appearance and a cross-sectional view of an ultrasonically welded terminal. This product uses ultrasonic terminal welding to bond copper terminals directly to the copper circuit pattern. In a conventional solder joint structure, the greatest amount of stress is concentrated in the solder layer due to difference in the coefficients of thermal expansion of the solder material and the copper material. As a result, failure may result whereby cracks form in the solder layer and the copper terminal is pulled out. Figure 7 shows a comparison of the results of copper terminal tensile strength tests before and after a thermal cycle test (test conditions: −40 to+150 °C repeatedly). For the conventional solder joint, an approximate 50% decrease in tensile strength from the initial value was confirmed after 300 cycles. On the other hand, almost no decrease in tensile strength was observed in the case of ultrasonic welding. This is because the copper terminals and the copper circuit pattern are bonded together directly with ultrasonic terminal welding, and there is no difference in the coefficients of thermal expansion at the joint surface.

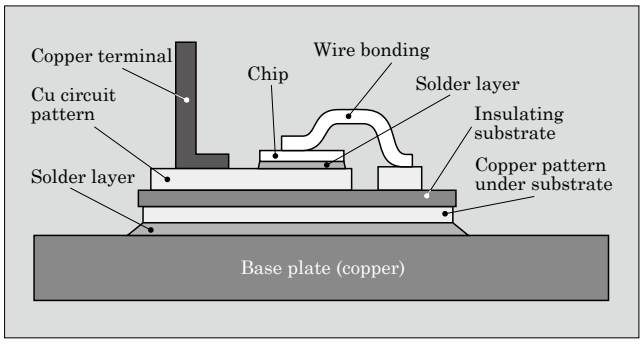

Fig.5 Cross-sectional schematic view of an IGBT module

Table 2 Technologies and materials applied to the V-Series HPM Family

PrimePACK™		HPM	
		Industrial use	Traction use
Terminal welding method	Ultrasonic welding	Solder welding	Solder welding
Insulating substrate	Al_2O_3	Si_3N_4	AlN
Solder material under insulating substrate	Sn-Sb	Sn-Pb	Sn-Pb
Base material Base thickness	Copper 3 mm	Copper 5 mm	AlSiC 5 mm

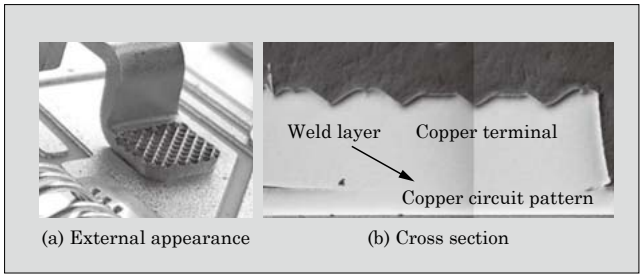

Fig.6 External appearance and cross-sectional view of ultrasonically welded terminal

4.2 Improved power cycling capability

As shown in Fig. 5, thermal cycle stress occasionally causes cracks to form in the solder layer between the copper base and the copper pattern under the substrate. With the PrimePACK™ series, tolerance to high temperature cycling is achieved by using highly

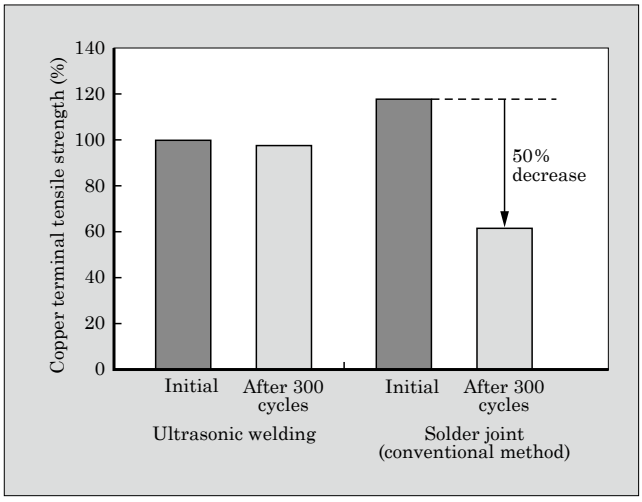

Fig.7 Copper terminal tensile strength test results

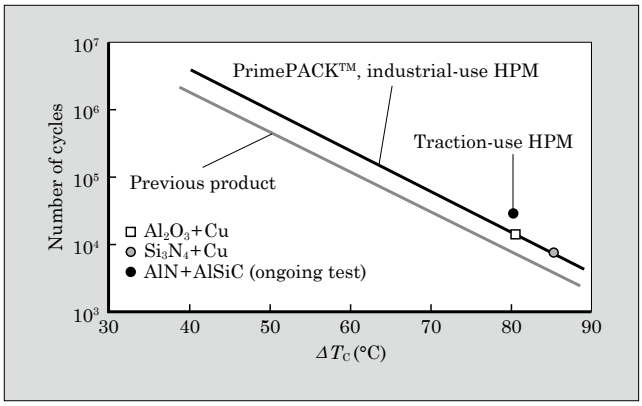

Fig.8 ΔT_C power cycling capability

crack-resistant Sn-Sb solder.

In traction-use HPMs, to ensure even higher reliability, an AlN substrate is used as the insulating substrate and an AlSiC base is used as the base material. AlSiC is a composite of Al and SiC, and having a coefficient of thermal expansion close to that of the AlN substrate, achieves higher thermal cycling capability and power cycling capability than in the case of a copper base. In the simulated tests of actual operation shown in Fig. 8, improved thermal cycling (ΔT_c power cycling) capability was realized. The V-Series HPM Family has a power cycle capability of greater than 10,000 cycles at ΔT_c=80 °C, and realizes more than twice the ΔT_c power cycling capability as the previous product.

4.3 Improved environmental durability of molded case

When the surface of a molded case is placed under a high electric field, dust and moisture adhering to the molded case surface cause the surface to become carbonized, and form a conductive path (track). This degrades the insulating performance and may lead to breakdown of the insulation. Wind and solar power generating equipment are often installed in high humidity environments containing large amounts of dust and salt. So that an IGBT module can be used in such an environment while maintaining high reliability, the development of a molded case on which a carbonized conductive path is not easily formed is needed. This product series uses a mold resin having a high comparative tracking index (CTI) of ≥ 600 to ensure high anti-tracking performance.

4.4 Reduction of internal inductance

The V-Series HPM Family introduced in Section 3 achieves electrical characteristics suitable for application in the high capacity field. Most power conversion equipment used in the high capacity field is required to be able to block large currents instantaneously. For this purpose, reducing the internal inductance L_m of the product to reduce the surge voltage is very important. In this product series, the collector and emitter terminals, which are main terminals, are located in close proximity to one another so as to actively utilize the mutual interactions of the magnetic field and reduce L_m.

5. Postscript

This paper has introduced the "V-Series HPM Family" which incorporates "V-Series" IGBTs and realizes significantly improved reliability. Fuji Electric is confident that these modules will be able to support the diverse needs of the high-power device field, as well as the needs of the renewable energy field for which a rapidly growing market is being formed.

Fuji Electric will continue to strive to advance the level of semiconductor technology and package technology so as to respond additional needs, and to develop new products that will contribute to the progress of power electronics.

References

(1) Yamamoto, T. et al. New High Power 2-in-1 IGBT Module. FUJI ELECTRIC REVIEW. 2011, vol.57, no.3, p.82-86.

(2) Nishimura, T. et al. High Power IGBT Modules. FUJI ELECTRIC REVIEW. 2009, vol.55, no.2, p.51-55.

(3) Takahashi, K. et al. New Lineup of V-Series IGBT Modules. FUJI ELECTRIC REVIEW. 2010, vol.56, no.2, p.56-59.

(4) Morozumi, A. et al. "Reliability of Power Cycling for IGBT Power Semiconductor Module." Conf. Rec. IEEE Ind. Appl. Conf. 36th. 2001. p.1912-1918.

New Lineup of Large-Capacity "V-Series" Intelligent Power Modules

Naoki Shimizu † **Tatsuya Karasawa** † **Kazumi Takagiwa** †

ABSTRACT

To meet the diversifying needs for power control, Fuji Electric has developed a family of large-capacity intelligent power modules (IPMs). These products with high-performance, new-generation IGBT chips, new control ICs and lower package inductance are able to reduce total power loss and radiated noise, and increase current capacity. A new solder material and divided direct copper bonding (DCB) are employed to enable a ΔTc power cycling capability significantly enhanced. Terminals and screw hole positions are compatible with existing products, allowing existing products to be replaced with the new products without major design changes.

1. Introduction[1][2]

Recently, as essential items for conserving energy and reducing CO_2 emissions in the industrial field, high efficiency power converting equipment is being used more and more. Additionally, the requirements for standard insulated gate bipolar transistor (IGBT) modules that integrate an IGBT chip and a free wheeling diode (FWD) chip into a single package are becoming more diverse. An intelligent power module (IPM) integrates a control IC for internal drive and protection functions into a standard IGBT module. With an IPM, optimized drive control can be performed so that the IGBT can be driven and provided with high reliability protection with low dissipation loss and low noise. IPMs are used in a wide range of applications, such as in motor driven equipment (numerical control (NC) machine tools, general-purpose inverters, servos, elevators, etc.), uninterruptible power supplies (UPS), power conditioning systems (PCS) for solar energy generation, and the like where low dissipation loss and low noise are strongly required.

Since beginning to commercialize IPMs in 1988, Fuji Electric has responded to market requests for lower power dissipation, lower noise and smaller size with each successive generation of devices. In recent years, through developing a "V-Series" IPM using a next-generation trench gate structure field stop (FS) type "V-Series" IGBT chip, even lower power dissipation loss and smaller size have been realized. This paper describes Fuji Electric's new lineup of large capacity "V-Series" IPMs and the large capacity series of IPMs (P631 package).

2. "V Series IPM" Product Lineup[1][2]

At present, Fuji Electric's V-Series of IPMs is available in the four packages (small capacity: P629, medium capacity small size: P626, medium capacity low profile: P630, large capacity: P631) as shown in Fig. 1. All of these packages comply with the RoHS

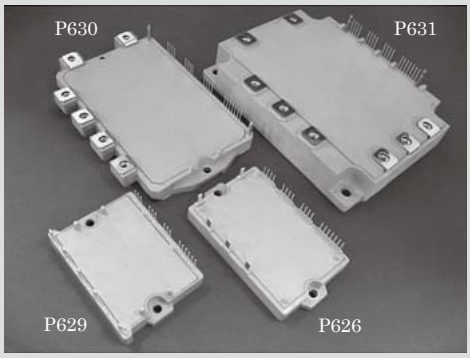

(a) Package appearance

P629 package	P626 package	P630 package	P631 package
L49.5×W70 ×H12.5 (mm)	L50×W87 ×H12 (mm)	L84×W128.5 ×H14 (mm)	L110×W142 ×H27 (mm)

(b) Type of package

Fig.1 Appearance of "V-Series" IPM packages

*1: RoHS directive: European Union (EU) directive on the restriction of the use of certain hazardous substances in electrical and electronic equipment

† Fuji Electric Co., Ltd.

directive*[1] Fuji Electric plans to expand further the V-Series IPM product lineup, increasing the capacity beyond that of the previous "R-Series" IPMs, to rated currents of 20-400 A for the 600 V rated voltage series, and to 10-200 A for the 1,200 V rated voltage series. In addition to the protective functions of overcurrent protection, short-circuit protection, control supply protection in control circuit and IGBT chip over heat protection, which are the same protective functions as had been provided previously, a cause identification function based on the width of the alarm output has been newly added. In the P629 package, the previous method of N-line current detection based on shunt resistance has been changed to a method of IGBT sense current detection, enabling protection in the case of a ground fault in which current flows only through the upper arm element.

Table 1 lists the product lineup and functions of the V-Series of IPMs.

3. Large-capacity "V-Series" IPM Product Overview

3.1 Development goals

Development goals for the large-capacity V-Series of IPMs are as follows.

(1) Reduction of total dissipation loss
(2) Improvement of tradeoff relation between switching loss and radiation noise
(3) Expanded current rating (400 A/600 V, 200 A/1,200 V)
(4) Shorter deadtime
(5) Separate alarm output signal for each cause
(6) Upper arm alarm output (P631: alarm control terminal added for upper arm)
(7) Maintain package compatibility (tapped hole locations, guide pins)
(8) Compliance with RoHS directive
(9) Reduction of internal inductance
(10) Improvement of ΔT_c power cycling capability

Table 1 "V-Series" IPM product lineup and functions

Rated voltage	Rated current	Product type		Internal functions*						Package model
				Both upper and lower arms				Upper arm	Lower arm	
		6-in-1	7-in-1	Drive	UV	TjOH	OC	ALM	ALM	
600 V	20 A	6MBP20VAA060-50	–	○	○	○	○	–	○	P629
	30 A	6MBP30VAA060-50	–	○	○	○	○	–	○	
	50 A	6MBP50VAA060-50	–	○	○	○	○	–	○	
	50 A	6MBP50VBA060-50	–	○	○	○	○	○	○	P626
	75 A	6MBP75VBA060-50	–	○	○	○	○	○	○	
	50 A	6MBP50VDA060-50	7MBP50 VDA060-50	○	○	○	○	○	○	P630
	75 A	6MBP75VDA060-50	7MBP75 VDA060-50	○	○	○	○	○	○	
	100 A	6MBP100VDA060-50	7MBP100 VDA060-50	○	○	○	○	○	○	
	150 A	6MBP150VDA060-50	7MBP150 VDA060-50	○	○	○	○	○	○	
	200 A	6MBP200VDA060-50	7MBP200 VDA060-50	○	○	○	○	○	○	
	200 A	6MBP200VEA060-50	7MBP200VEA060-50	○	○	○	○	○	○	P631
	300 A	6MBP300VEA060-50	7MBP300VEA060-50	○	○	○	○	○	○	
	400 A	6MBP400VEA060-50	7MBP400VEA060-50	○	○	○	○	○	○	
1,200 V	10 A	6MBP10VAA120-50	–	○	○	○	○	–	○	P629
	15 A	6MBP15VAA120-50	–	○	○	○	○	–	○	
	25 A	6MBP25VAA120-50	–	○	○	○	○	–	○	
	25 A	6MBP25VBA120-50	–	○	○	○	○	○	○	P626
	35 A	6MBP35VBA120-50	–	○	○	○	○	○	○	
	50 A	6MBP50VBA120-50	–	○	○	○	○	○	○	
	25 A	6MBP25VDA120-50	7MBP25VDA120-50	○	○	○	○	○	○	P630
	35 A	6MBP35VDA120-50	7MBP35VDA120-50	○	○	○	○	○	○	
	50 A	6MBP50VDA120-50	7MBP50VDA120-50	○	○	○	○	○	○	
	75 A	6MBP75VDA120-50	7MBP75 VDA120-50	○	○	○	○	○	○	
	100 A	6MBP100VDA120-50	7MBP100VDA120-50	○	○	○	○	○	○	
	100 A	6MBP105VEA120-50	7MBP100VEA120-50	○	○	○	○	○	○	P631
	150 A	6MBP150VEA120-50	7MBP150VEA120-50	○	○	○	○	○	○	
	200 A	6MBP200VEA120-50	7MBP200VEA120-50	○	○	○	○	○	○	

* : Drive: IGBT drive circuit, UV: Control supply undervoltage protection, TjOH: IGBT chip over heat protection, OC: Overcurrent protection, ALM: Alarm output

3.2 Characteristics[1][2]

(1) Reduction of total dissipation loss

To improve equipment controllability, as is requested by customers, the IPM dissipation loss must be reduced in order to realize a higher carrier frequency and larger output current. Moreover, a reduction in dissipation loss enables the cooling system for the equipment to be simplified, such as with smaller-sized air-cooling fins and fans, and also contributes to a lower overall low cost of the equipment.

Figure 2 compares the total dissipation loss during PWM inverter operation for a V-Series IPM and the previous product (R-Series IPM), both of which are 300 A/600 V devices. The V-Series IPM realizes at least 20% lower dissipation loss than the previous product.

With the V-Series IPM, in the case of a 300 A/600 V device, the static loss P_{sat} and the turn-off loss P_{off} of the IGBT account for approximately 50% of the total dissipation loss during inverter operation. The on-voltage $V_{CE(sat)}$ and turn-off loss E_{off} characteristics that determine these two types of loss have a tradeoff relationship with the short-circuit withstand capability of the IGBT. Improving the tradeoff is a key point for reducing the dissipation loss. V-Series IGBT chips for standard IGBT modules feature an optimized surface structure to reduce the resistance of the drift layer and make the chip thinner, thereby lowering $V_{CE(sat)}$ and improving E_{off}[3]. On the other hand, IGBT chips for V-Series IPMs feature an even finer surface structure and an improved tradeoff relationship with $V_{CE(sat)}$ and E_{off}[4]. As a result of the finer structure, however, because $V_{CE(sat)}$ decreases and the current flows with greater ease, short-circuit current will increase and the short-circuit withstand capability (allowable time) will decrease. Therefore, a chip that features an improved tradeoff relationship between $V_{CE(sat)}$ and E_{off} can be used to speed up the short-circuit protection function.

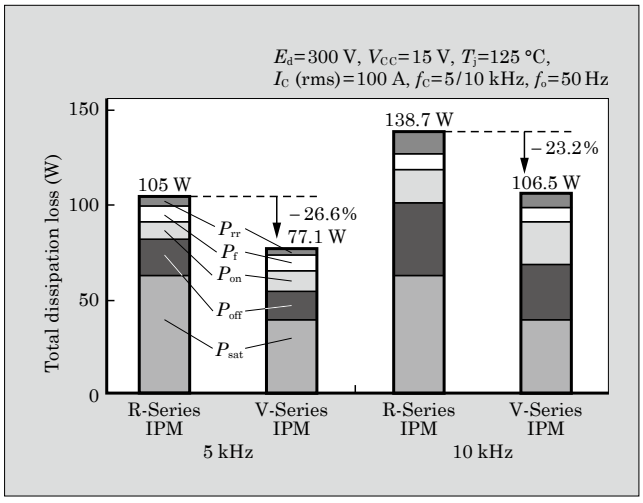

Fig.2 Comparison of total dissipation loss in 300 A/600 V products

For the 600 V series, because the rated current is larger and the difference between rated voltage and working voltage is smaller than the 1,200 V series, the design must take into consideration the surge voltage. In addition to reducing the internal impedance of the package, as will be described later, by shifting the $V_{CE(sat)}$ and E_{off} tradeoff to the low $V_{CE(sat)}$ side where the turn-off di/dt is smaller, the device was optimized so that the surge voltage would be equivalent to that of previous products.

(2) Improvement of tradeoff relation between switching loss and radiation noise

A tradeoff relationship exists between switching loss and radiation noise. To improve this relationship, the internal capacitance of the IGBT was reduced, the temperature dependence of the control IC was improved, and the internal circuit wiring pattern of package was optimized[5]. As a result, in a relative comparison of radiation noise using inverter test equipment, the peak radiation noise in a 300 A/600 V product was reduced by approximately 3 dB compared to the previous product as is shown in Fig. 3.

(3) Expanded current rating (400 A/600 V, 200 A/1,200 V)

With the V-Series large-capacity IPM (P631), the two power chips (IGBT and FWD) used in parallel in the R-Series large-capacity IPM (P612) are integrated into a single chip, and the chip size is miniaturized and optimized to reduce the total area of the 300 A/600 V power chip by 32%. By configuring the control circuit as a two-level structure positioned above the power unit, the product series could be expanded to 400 A/600 V and 200 A/1,200 V in an package of equivalent size and having the same mounting position as previous products. This was a first in the industry.

(4) Shorter deadtime

For the purpose of preventing upper and lower arm short circuits, the inverter control is provided with a deadtime interval. Shortening the deadtime interval is important for improving waveform distortion and rotational unevenness. With V-Series IPMs, the control IC switching time has been optimized and temperature dependence has been improved to reduce the minimum deadtime interval to 1 μs from the previous value of 2.4

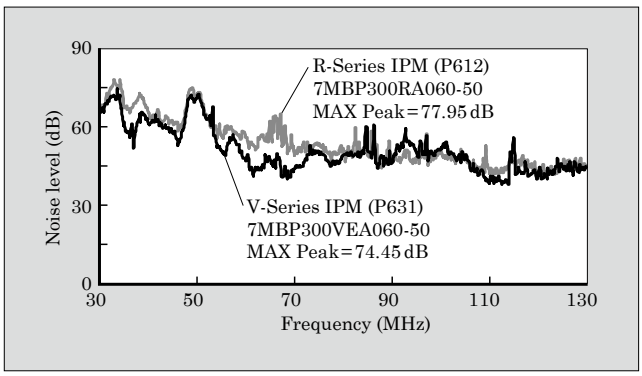

Fig.3 Comparison of radiation noise

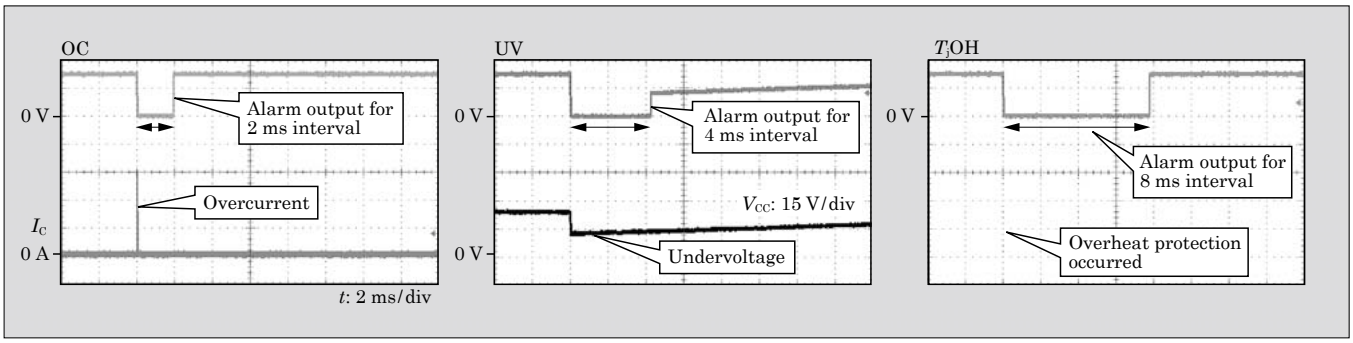

Fig.4 Alarm cause identification function

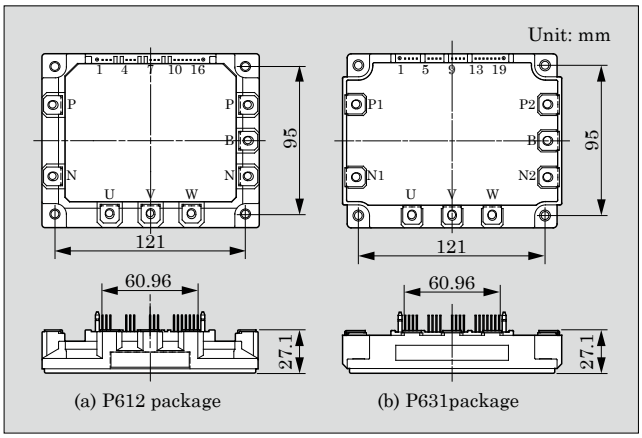

Fig.5 Package dimensions

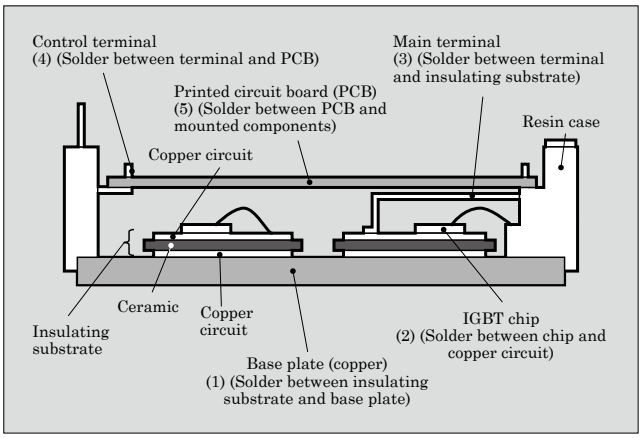

Fig.6 Internal structure of P631 package

μs.

(5) Separate alarm output signal for each cause

With V-Series IPMs, the widths of outputted alarm pulses differ according to the alarm cause (see Fig. 4). As a result, the cause of the protective alarm can be identified easily, and after the equipment has been stopped by the IPM alarm, cause analysis and restoration can be performed in a shorter amount of time.

4. Package

4.1 Package dimensions

Figure 5 shows the dimensions of the P631 and P612 packages. The P631 is provided with the same mounting holes, terminal locations and height dimensions as the existing P612, and maintains package compatibility when being installed in equipment. Additionally, an alarm output terminal has been added to each phase of the upper arm, and the terminal pitch and total width of the control terminals was made common.

4.2 Compliance with RoHS directive

Figure 6 shows the internal structure of the P631 package. In a conventional IPM, lead is used primarily at soldering locations. Solder material is used at five locations: (1) the junction between the insulating substrate and base plate, (2) the junction between the chip and copper circuit, (3) the junction between main terminals and the insulating substrate, (4) the junction between control terminals and the printed circuit board, and (5) the junction between the printed circuit board and mounted components. The P631 uses lead-free solder at all of these locations, and is compliant with the RoHS directive.

4.3 Reduction of inductance

Figure 7 shows a schematic drawing of the internal wiring, and Fig. 8 compares the results of measurement of the internal inductances of the P631 and P612 packages. Aiming to reduce internal inductance through the mutual inductance effect, a parallel plate configuration employing overlapping P and N line terminal bars was used. As a result, the internal inductance is reduced by approximately 22% compared to the P612 package, and an effect is obtained whereby the radiation noise is lower and the turn-off surge does not become excessive, as described in Section 3.

4.4 Improvement of ΔT_c power cycling capability

IGBT modules are typically formed by soldering together a base having a heat dissipating surface and an insulated circuit board. Because these materials have different coefficients of thermal expansion, stress is repeatedly generated in the soldered junction between the materials whenever the temperature changes. In a ΔT_c power cycling test in which the case temperature was varied, it was confirmed that solder in the junction

between the insulating substrate and the base plate will crack, expand and ultimately break.

With the P631 package, the insulating substrate has been subdivided and miniaturized to ease the stress on the solder. Additionally, the solder material used in the junction between the insulating substrate and the base plate has been changed to material having higher mechanical strength. As a result, ΔT_c power cycling capability at ΔT_c=80 K has been improved by more than twice as that of the P612.

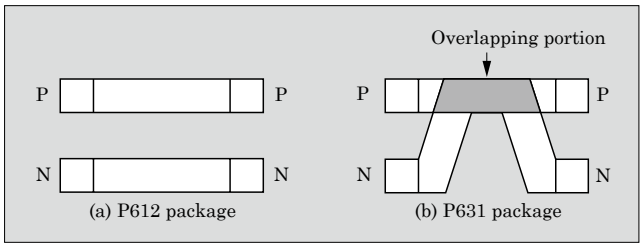

Fig.7 Schematic of internal wiring in package

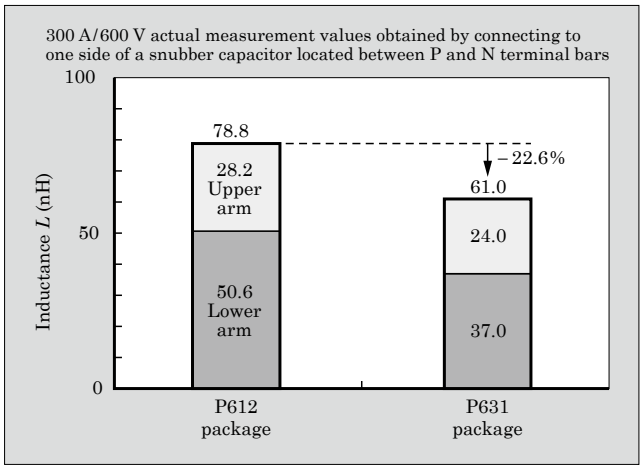

Fig.8 Comparison of results of internal inductance measurement

5. Postscript

This paper has described Fuji Electric's new lineup of large-capacity "V-Series" IPMs and the large-capacity series of IPMs (P631 package). The V-Series of IPMs realize low power dissipation, low noise and RoHS compliance, as requested in the marketplace, and also provide such value-added features as larger capacity, shorter deadtime, an alarm cause identification function, and package compatibility.

In the future, Fuji Electric intends to continue to improve the performance and expand the lineup of available packages, and will focus on developing products capable of contributing to the conservation of energy and protection of the environment.

References

(1) Motohashi, S. et al. "The 6th Gen. Intelligent Power Module," in Proc. 2011 PCIM, p.161-166.
(2) Shimizu, N. et al. V Series' Intelligent Power Modules. FUJI ELECTRIC REVIEW. 2010, vol.56, no.2, p.60-64.
(3) Kobayashi, Y. et al. "The New concept IGBT-PIM with the 6th generation V-IGBT chip technology," in Proc. 2007 PCIM.
(4) Momose, M. et al. "A 600 V Super Low Loss IGBT with Advanced Micro-P Structure for the next Generation IPM," in Proc. 2010 ISPSD.
(5) Onozawa, Y. et al. "Development of the next generation 1200 V trench-gate FS-IGBT featuring lower EMI noise and lower switching loss," in Proc. 2007 ISPSD, p.13-16.

Hybrid Si-IGBT and SiC-SBD Modules

Masayoshi Nakazawa † **Toshiyuki Miyanagi** † **Susumu Iwamoto** †

ABSTRACT

Fuji Electric has developed hybrid modules that combine silicon-insulated gate bipolar transistor (Si-IGBT) and silicon carbide-Schottky barrier diode (SiC-SBD) for high-efficiency inverter applications that contribute to energy savings. The SiC-SBD chip was developed jointly with the National Institute of Advanced Industrial Science and Technology, a public research institute, and the Si-IGBT chips are the latest 6th-generation "V-Series" IGBTs from Fuji Electric. The product lineup are 600 V class rated at 50/75/100 A, and 1,200 V class rated at 35/50 A. Inverter power loss in the 1,200 V 50 A class has been reduced by 23% compared to the V-series module.

1. Introduction

To prevent global warming, the further reduction of greenhouse gases (such as CO_2) is a pressing issue. The greatest benefit of using power electronics technology to reduce greenhouse gases is that electrical power becomes more energy-efficient. In such an undertaking, increasing the efficiency of inverters is an important factor. To do so requires technical innovation of the power devices, circuits, controllers and other components used in inverters. Since power devices are the main elements used in inverters, there is increasing demand for low loss power devices that realize higher efficiency. The insulated gate bipolar transistor (IGBT) is such a power device, and the use of silicon (Si) IGBT and free wheeling diode (FWD) chips is common. However, Si semiconductor device performance is approaching its theoretical limits based on its material properties, and future breakthroughs that achieve significantly lower loss cannot be expected. For this reason, wide bandgap (WBG) semiconductors, which exhibit material properties superior to those of Si semiconductors, are promising.

Fuji Electric is advancing the development of silicon carbide (SiC) semiconductor devices, which are a type of WBG semiconductors. With an SiC device, higher breakdown voltage and lower on-state resistance can be achieved than with a Si device. In theory, the on-state resistance of a SiC can be made lower than that of a Si device having the same breakdown voltage. For this reason, SiC devices do not necessarily need to be bipolar devices as was essential for reducing the on-state resistance in high-voltage Si devices. Bipolar devices are associated with the injection of minority carriers and generally exhibit greater switching energy than unipolar devices. Thus, unipolar devices are desirable for reducing the switching energy. Accordingly, the use of a SiC unipolar device enables low on-state resistance and low switching energy to be achieved simultaneously.

2. Product Overview

Figure 1 shows an internal circuit diagram of a power integrated module (PIM). Si-IGBT and silicon carbide schottky barrier diode (SiC-SBD) hybrid modules, which enabled to reduce power loss than ever before, have been developed using SiC-SBD unipolar devices as FWDs. A chip developed in collaboration with the National Institute of Advanced Industrial Science and Technology is used as the SiC-SBD, and Fuji Electric's latest chip, a 6th generation "V-Series" IGBT chip is used as the Si-IGBT.

Figure 2 shows the appearance, and Table 1 lists the product lineup of the Si-IGBT and SiC-SBD hybrid modules. For high efficiency inverter applications, 50 A, 75 A and 100 A rated products have been de-

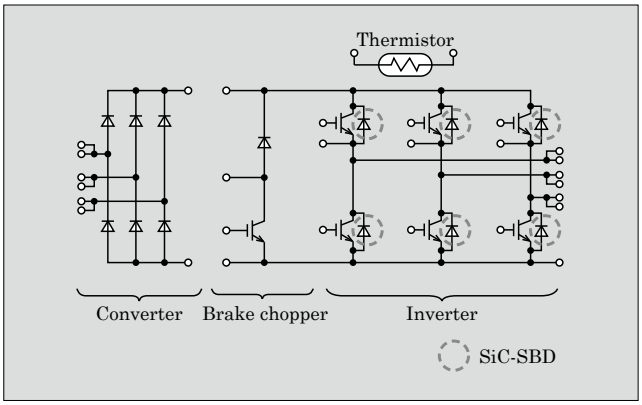

Fig.1 PIM internal circuit diagram

† Fuji Electric Co., Ltd.

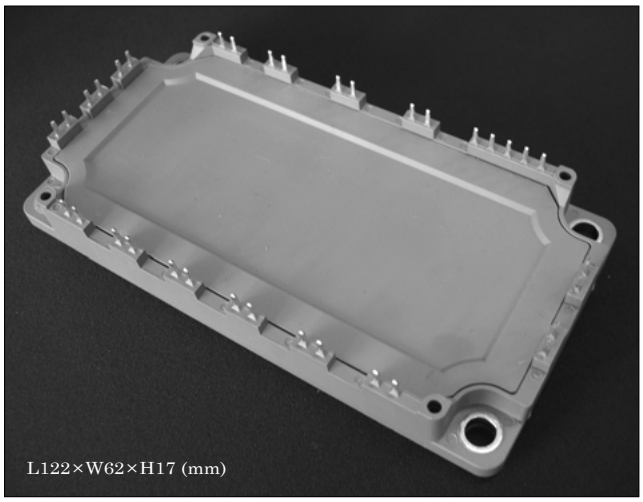

Fig.2 Appearance of the hybrid Si-IGBT/SiC-SBD module

Table 1 Lineup of hybrid Si-IGBT/SiC-SBD modules

Rated voltage (V)	Rated current (A)	Hybrid module model
600	50	7MBR50VB060S-50
	75	7MBR75VB060S-50
	100	7MBR100VB060S-50
1,200	25	7MBR25VB120S-50*
	35	7MBR35VB120S-50
	50	7MBR50VB120S-50

∗ : To Be Determined

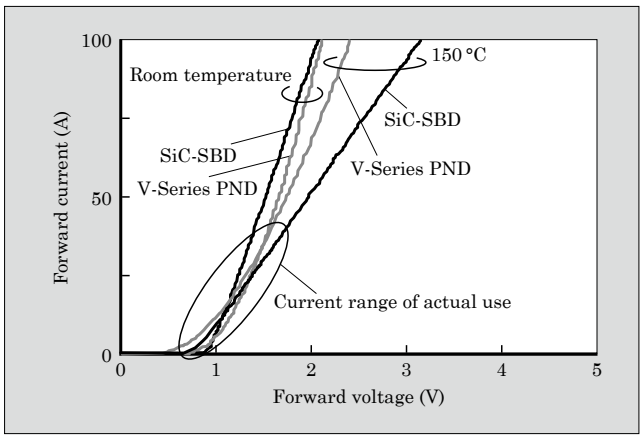

Fig.3 Forward characteristics

veloped for the 600 V series, and 35 A and 50 A rated products have been developed for the 1,200 V series. Product performance and characteristics are presented below for the 1,200 V/ 50 A product, as a representative example.

3. Static Characteristics

3.1 Forward characteristics

Figure 3 shows the forward characteristics of a SiC-SBD and a V-Series PN junction diode (V-Series PND), and Fig. 4 shows the temperature characteristics of the

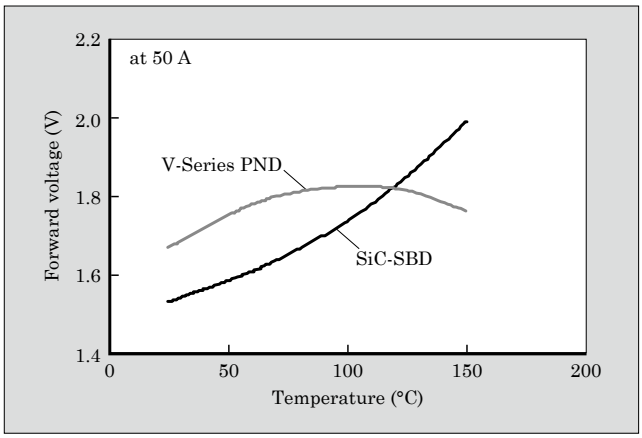

Fig.4 Temperature characteristics of the forward voltage

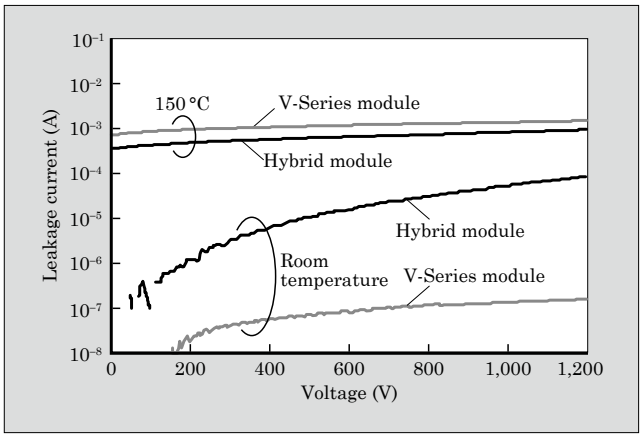

Fig.5 Leakage current characteristics

forward voltage V_f at the rated current of 50 A. In the current range that is actually used, the V_f of the SiC-SBD is the same as that of the V-Series PND. From Fig. 4, it can be seen that at temperatures higher than 100 °C, the V-Series PND exhibits a negative temperature coefficient with reducing V_f. A device with a negative temperature coefficient is prone to current imbalance when in a multi-parallel connection. On the other hand, the SiC-SBD, which has a strong positive temperature characteristic, is unlikely to create a current imbalance, even when in a multi-parallel connection.

3.2 Leakage current characteristics

Figure 5 compares the leakage current characteristics of the hybrid module and a V-Series module. The leakage current of the hybrid module is about 1,000 times as large as that of the V-Series module when at room temperature, but is only slightly less than that of the V-Series module when at 150 °C. As shown in Fig. 6, the leakage current of the hybrid module is nearly constant at temperatures of around 100 °C and below, and increases similarly as the V-Series at higher temperatures. The SiC-SBD, which has a wide bandgap and therefore very few thermally excited carriers, is less affected by temperature rise. The increase in leakage current at temperatures above 100 °C is a result of

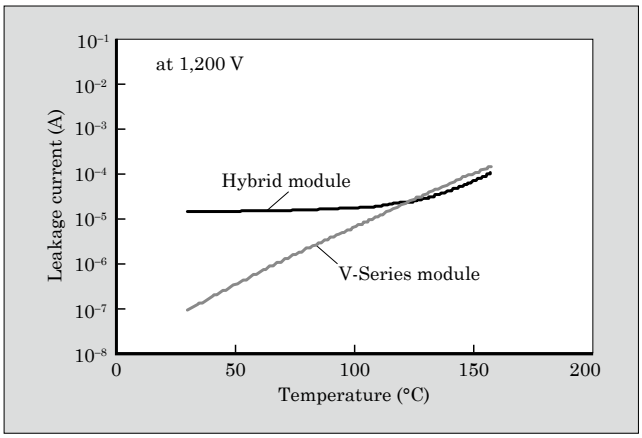

Fig.6 Temperature characteristics of leakage current

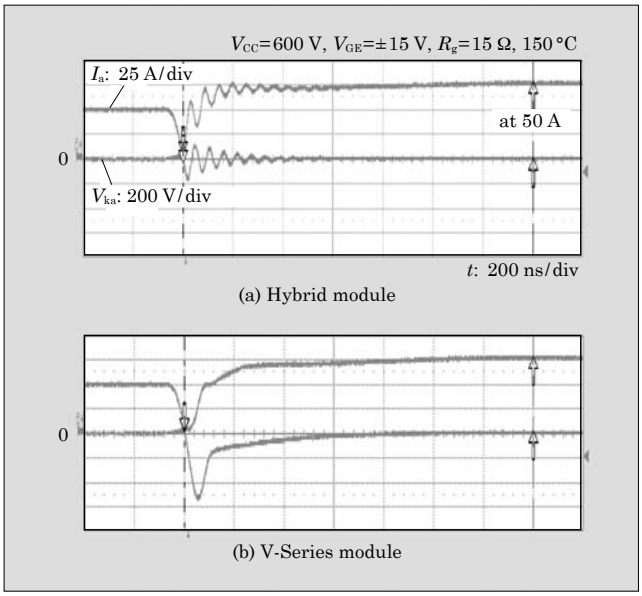

Fig.7 Reverse recovery waveforms

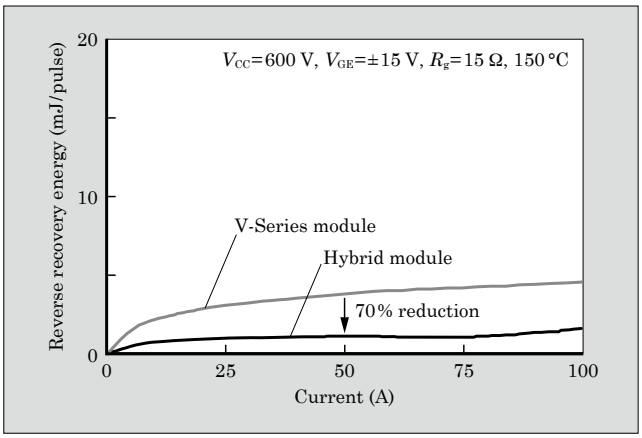

Fig.8 Current characteristic of reverse recovery loss

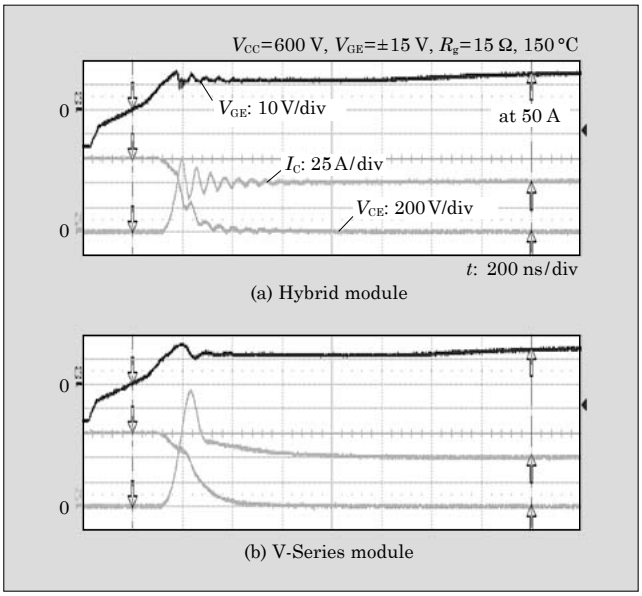

Fig.9 Turn-on waveforms

the leakage current of the IGBT becoming dominant. Thus, even if the SiC-SBD exhibits a large leakage current at room temperature, because its leakage current during high temperature operation is the same as that of a V-Series device, the SiC-SBD is similarly able to operate at junction temperatures of up to 175 °C.[1]

4. Switching Characteristics

4.1 Reverse recovery characteristics

Figure 7 compares reverse recovery waveforms of the hybrid module and a V-Series module. The hybrid module exhibits extremely lower reverse recovery peak current. This behavior can be explained from little injection of minority carriers since the SIC-SBD is a unipolar device. As can be seen in Fig. 8, at the rated current of 50 A, reverse recovery energy can be reduced significantly by 70% compared to the V-Series module.

4.2 Turn-on characteristics

The reverse recovery peak current of the FWD is reflected in the turn-on peak current of the IGBT in the opposing arm, and a reduction in turn-on energy can be attained as a result of the reduction in reverse recovery energy.

Figure 9 compares turn-on waveforms of the hybrid

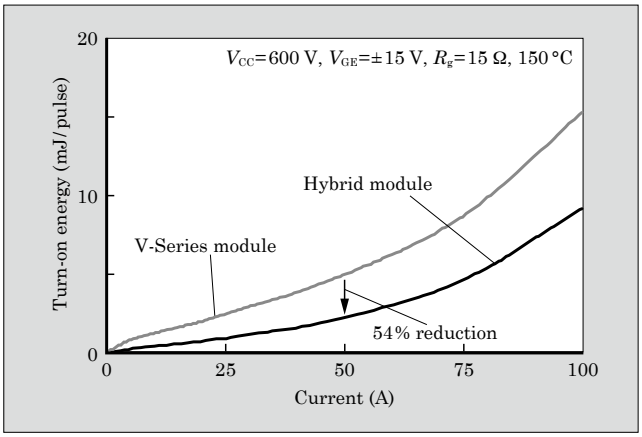

Fig.10 Current characteristics of turn-on energy

module and V-Series module. As in the reverse recovery waveform, there is extremely lower current peak. At the rated current of 50 A, as is shown in Fig. 10, the turn-on energy can be reduced significantly by 54% compared to the V-Series module.

4.3 Turn-off characteristics

Figure 11 shows a comparison of the turn-off waveforms of the hybrid module and V-Series module. At the rated current of 50 A, the turn-off surge voltage of the hybrid module is 47 V lower than that of the V-Series module. In general, the surge peak voltage can be defined by Equation (1), and if the IGBT element characteristics and the main circuit inductance are equivalent, the difference in the surge voltages is originated from the difference of the transient on-state voltages of the diodes. Figure 12 compares transient on-state waveforms of the diodes. Because the drift layer of the SiC-SBD has a much lower resistance

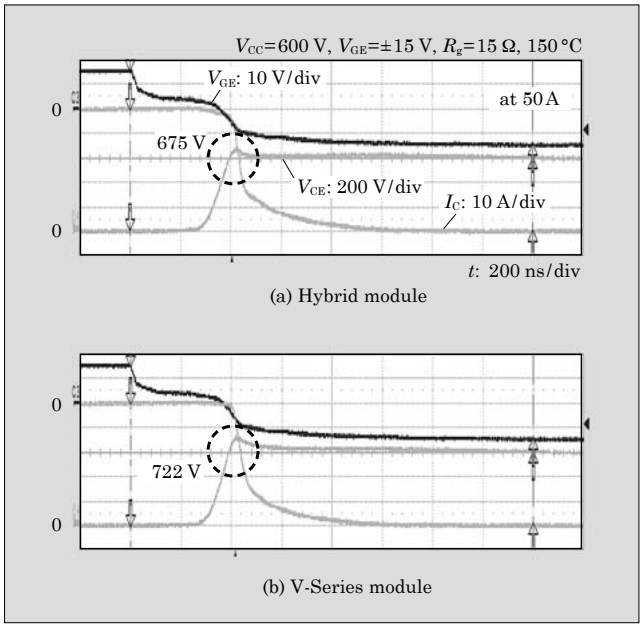

Fig.11 Turn-off waveforms

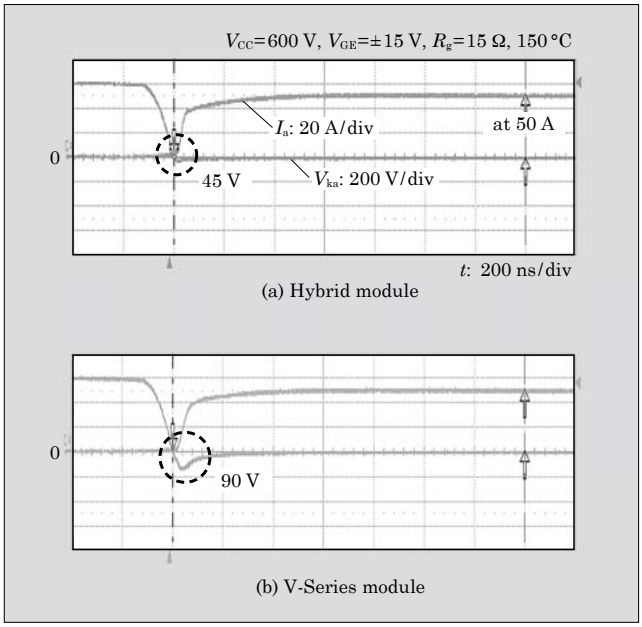

Fig.12 Diode transient on-state recovery waveforms

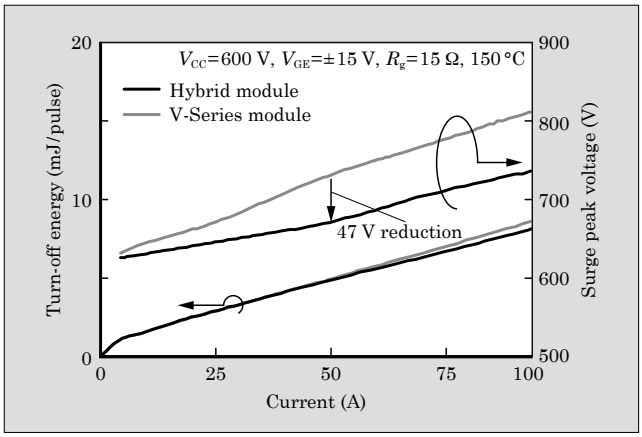

Fig.13 Turn-off energy and surge peak voltage/current characteristics

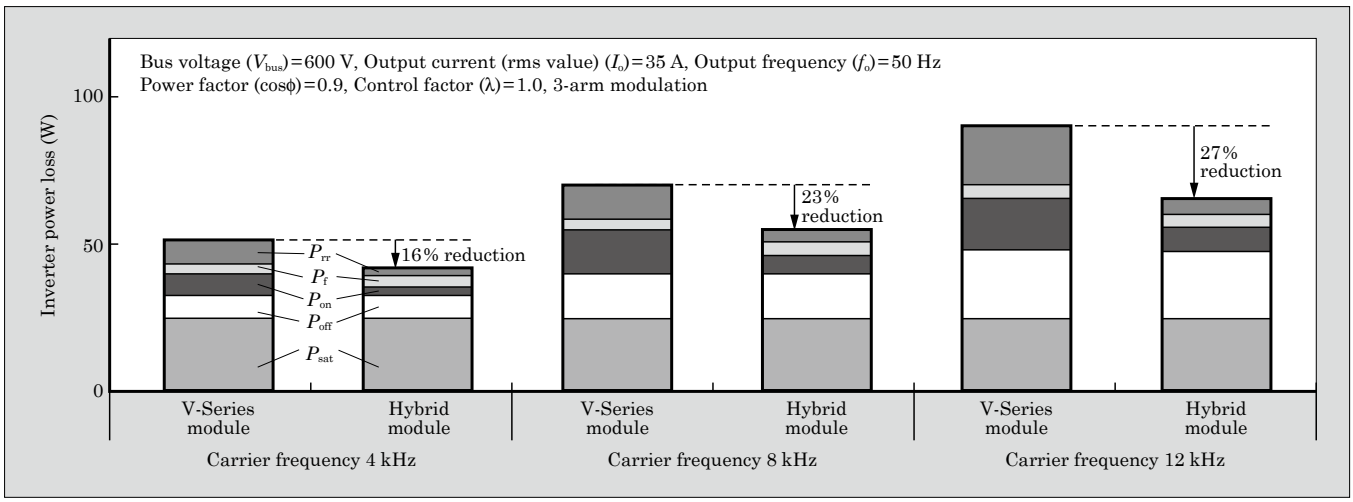

Fig.14 Inverter power loss

than that of the V Series PND, the transient on-state voltage of the SiC-SBD is reduced from 90 V to 45 V. Therefore, as shown in Fig. 13, the surge voltage at turn-off can be kept low and the turn-off energy can be reduced.

$$V_{Sp} = V_{CC} + L_s \cdot \frac{dI_C}{dt} + V_{TR} \quad \cdots\cdots(1)$$

V_{Sp} : Surge peak voltage
V_{CC} : Applied voltage
L_s : Inductance of main circuit
I_C : Collector current
V_{TR} : Transient on-state voltage

5. Inverter Power Loss

Figure 14 shows the calculated results of inverter power loss in the newly developed hybrid module and the V-Series module. When the carrier frequency is 8 kHz, the total power loss of the hybrid module can be reduced significantly by 23% for that of the V-Series module. Moreover, because the rate of loss reduction increases with hisher carrier frequency, the hybrid module is more effective for applications involving high frequency operation.

6. Postscript

This paper introduced the Si-IGBT and SiC-SBD hybrid module that combines a SiC-SBD, developed in collaboration with the National Institute of Advanced Industrial Science and Technology, and a 6th generation "V-Series" IGBT chip, which is Fuji Electric's latest chip. By greatly reducing the power loss of the device itself, this product is expected to contribute significantly to the achievement of higher efficiency inverters. In the future, Fuji Electric intends to expand the lineup of products that use SiC chips, and to contribute to efforts for preventing global warming.

The authors wish to thank all parties concerned at the Advanced Power Electronics Research Center of the National Institute of Advanced Industrial Science and Technology (AIST) for their cooperation in the development of the SiC-SBD chip. A portion of this development work was carried out under the AIST Industrial Transformation Research Initiative "SiC Device Practical Application Verification Based on Mass Production Prototype" in fiscal years 2008, 2009 and 2010.

References

(1) Takahashi, K. et al. New Lineup of V-Series IGBT Modules. FUJI ELECTRIC REVIEW. 2010, vol.56, no.2, p.56-59.

Packaging Technologies for SiC Power Modules

Masafumi Horio † **Yuji Iizuka** † **Yoshinari Ikeda** †

ABSTRACT

Wide bandgap materials such as silicon carbide (SiC) and gallium nitride (GaN) are attracting attention as materials for next-generation power semiconductor devices. Fuji Electric is currently developing new packaging technologies to take full advantage of SiC devices. Compact and highly reliable power modules with low thermal resistance and high-temperature operating capability can be realized by replacing aluminum wire bonding, solder joints and silicone gel encapsulating structures with copper pin connections, silver sintering joints and epoxy resin molding structures. Improved performances of prototype all-SiC modules and SiC diode modules with new packaging technologies have been evaluated.

1. Introduction

Recently, power modules have been widely used in industrial, consumer products and hybrid and electric vehicle applications. As the performance of Si devices used in the power modules is approaching its theoretical limits, wide bandgap (WBG) devices such as silicon carbide (SiC) and gallium nitride (GaN) are attracting attention. WBG devices have some advantages such as higher dielectric breakdown voltage, lower loss, higher switching and higher temperature operation capability compared to Si devices.

This paper introduces new packaging technologies that take full advantage of the features of WBG devices, especially SiC devices.

2. Features and technology of SiC Power Module Package

Fuji Electric is presently evaluating SiC metal-oxide-semiconductor field-effect transistors MOSFETs and SiC Schottky barrier diodes (SBDs) to be implemented in SiC modules. New packaging technology introduced in this paper can also be applied to other SiC devices such as SiC insulated gate bipolar transistors (IGBTs).

Figure 1 shows the aluminum wire bonding structure, which is currently the mainstream structure for power modules, and the newly developed package structure.

In the conventional structure, the main current paths are formed from aluminum bonding wires and the direct copper bonding (DCB) substrate. On the other hand, in the newly developed structure, circuit paths are formed from a DCB substrate, a power board and Cu pins instead of bonding wires. Additionally, this new structure uses epoxy resins as the encapsulating material instead of silicone gel. The features and technologies of new structure that uses these new materials will be discussed below.

2.1 Downsizing

Power modules are being made smaller and smaller with the rise in power density of power chips and the reduction of thermal resistance resulting from improved packaging technology. In the conventional structure, aluminum wire requires a certain amount of area for bonding. Large current capacity power

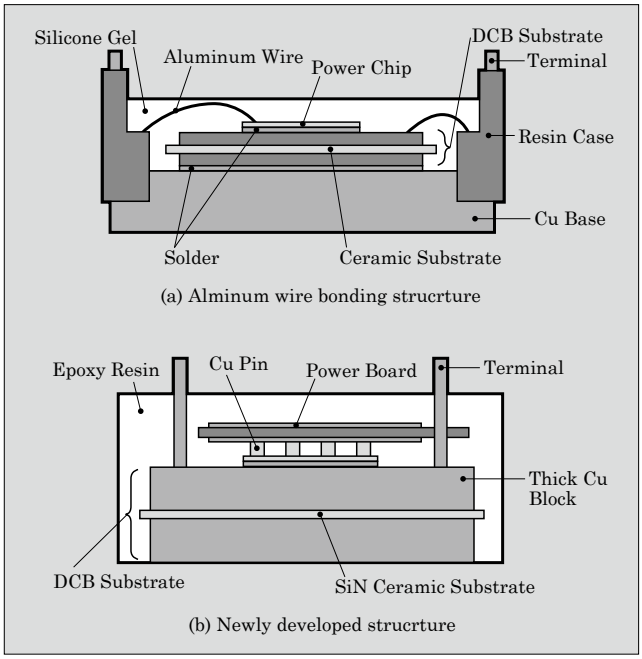

Fig.1 Comparison of power module structure

† Fuji Electric Co., Ltd.

modules require larger number of wires and result in many aluminum wires on the DCB substrate. This is a barrier to realize the high-density packaging i.e. the downsizing of power modules.

In the newly developed structure, Cu pins are used to connect power board to power chips, instead of using aluminum wires. The power board has a printed circuit board structure and current flows through its Cu pattern and Cu pins.

Because this structure allows current to flow in a vertical direction with respect to a power chip, power chips can be located close to each other. Furthermore, two layers of current paths, on both the DCB substrate and the power board, contribute to downsizing of the power module.

2.2 Low thermal resistance

In order to downsize power modules having high power density and to prevent temperature rise of the power chips, the thermal resistance of the power module package must be reduced. An alumina ceramic substrate is generally used in conventional structure shown in Fig. 1. This alumina ceramic acts as a large thermal barrier in the conventional structure due to its low thermal conductivity of about 20 W/(m·K). In order to reduce this large thermal resistance of the alumina ceramic, various developments have been undertaken.[(1),(2)]

In the development of this new structure, a much thicker Cu block is bonded to the silicon nitride (SiN) ceramic substrate in order to realize a further reduction of thermal resistance. The reason why a SiN ceramic substrate is used is because SiN has a larger thermal conductivity than alumina ceramic as well as large strength to endure the stress that occurs with thick Cu block during the thermal cycle. Figure 2 compares the power module thermal resistance of the conventional alumina ceramic structure with that of the newly developed SiN ceramic structure, when implemented with the same size power chips. The thermal resistance of the ceramic substrate in the new structure is one-fourth that of the conventional structure. The new structure enables a 50% reduction in the thermal resistance of the overall structure.

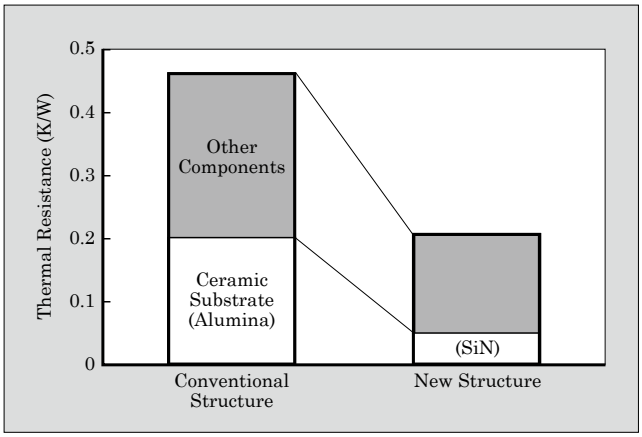

Fig.2 Comparison of power module thermal resistance

*1: The solidus line temperature is the temperature at which alloyed metal starts to melt, and the liquidus line temperature is the temperature at which alloyed metal melts completely. For pure metal, these temperatures are the same, and are called the melting point.

2.3 High temperature operation

One of the advantages of SiC devices is the capability to operate at high temperature. When a power chip can operate at high temperature, the cooling cost can be reduced and the overall system size can be reduced as a result of a downsized cooling system. In order to realize high temperature operation, it is necessary to improve the high temperature withstanding capability of the packaging components, especially the bonding material and the encapsulating material.

Currently, a tin (Sn)-silver (Ag) compound of lead (Pb)-free solder is generally used in power modules. The solidus line temperature*1 of that solder is below 250 °C. Because higher temperatures generally cause solder to deteriorate more quickly, a higher solidus temperature and melting point are preferred. However, a high temperature process would cause large stress and strain in the components. In order to reconcile these contradicting issues, Ag-sinter material is now being developed to apply as a bonding material. Figure 3 shows a cross-sectional view of the bonding area with Ag-sinter material.

Ag-sinter material exhibits superior characteristics and is capable of bonding under relatively low temperatures (ca. 300 °C) and has a high melting point of ca. 962 °C that is the same as Ag bulk material after sintering. Also, its thermal conductivity is larger by one digit than that of Sn-Ag compound solder.

Regarding encapsulating material, conventional silicone gel can withstand the duration of the lifetime (generally 10 years) of a power module at temperatures below 150 °C, but has difficulty in enduring if the operating temperature increases. Therefore, the newly developed structure uses a new epoxy resin that has glass transition temperature of over 200 °C.

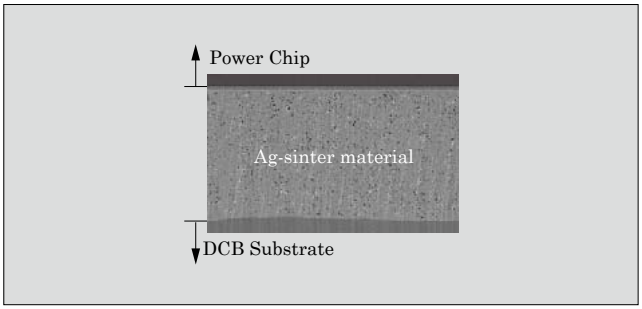

Fig.3 Cross-sectional view of Ag-sinter bonding area

2.4 High reliability

Improved reliability at high temperature is needed in order to realize high temperature operation of the power modules using SiC devices. The primary factors affecting the reliability of a power module having a conventional structure are the lifetime of the bonding area between aluminum wire and power chip electrodes, and the lifetime of the solder layer.[3] With the new structure, because aluminum wires are replaced by Cu pins, the factors affecting reliability are different from those of the conventional structure. A power cycling test, an important reliability test for power modules, was carried out with Si devices to compare reliability with that of the conventional structure. Figure 4 compares the power cycling capability of the new structure and the conventional structure.

This test results shows that the new structure has more than 30 times the power cycling capability as compared to the conventional structure under the conditions of chip junction temperature swings (ΔT_j) of 125 K and 150 K. One of the reasons for the improvement in power cycling capability is the epoxy resin molding structure. Figure 5 compares the stress occurring at the bonding material underneath the power chip in the cases of silicone gel and epoxy resin (result of FEM analysis). The vertical axis in Fig. 5 shows the values of stress occurring at the bonding material underneath power chip with silicone gel structure as 100.

This results shows that the epoxy molding structure reduces the stress at the bonding material by about half. It is speculated that the epoxy resin molding structure suppresses deformation of the power chips and the DCB substrate, for which expansion and constriction are repeated freely in silicone gel structure. A thermal cycling test was also carried out under the temperature range between −40 °C and 150 °C, and the results show that the new structure has a greater than 3,000 cycle capability.

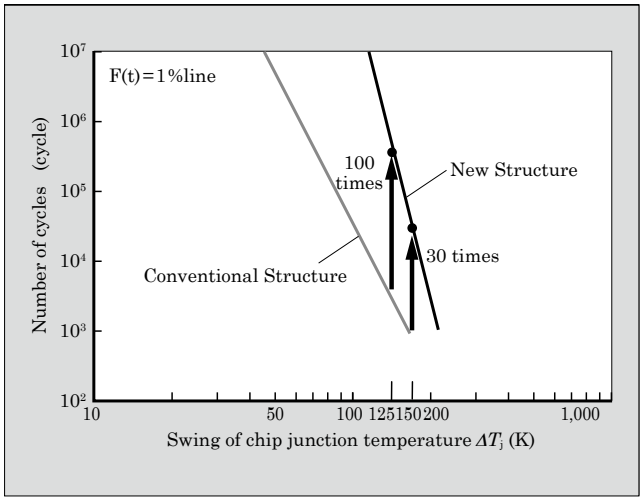

Fig.4 Comparison of power cycling capability

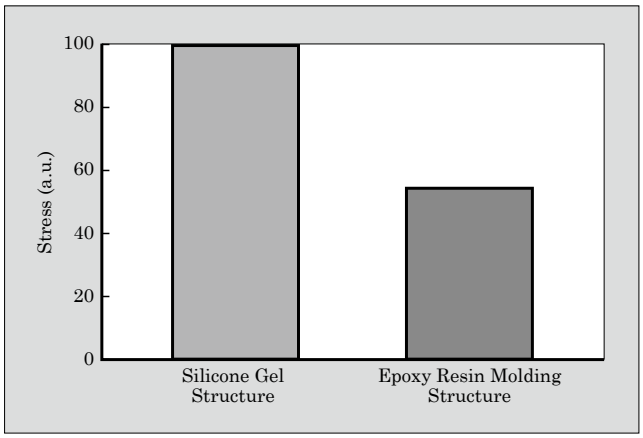

Fig.5 Comparison of stress occuring at bonding material underneath power chips

3. Prototype Modules with New Structure

The following two types of prototype modules were designed with the new structure that realizes downsizing, low thermal resistance, high temperature operation and high reliability.[4]~[6]

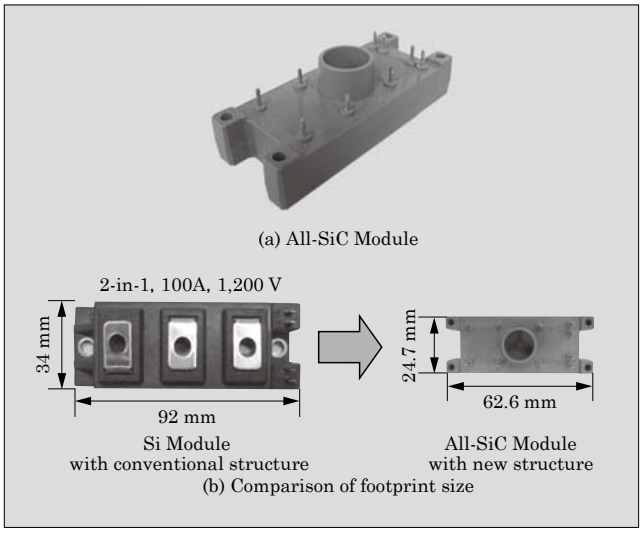

Fig.6 External view of All-SiC module and its footprint size

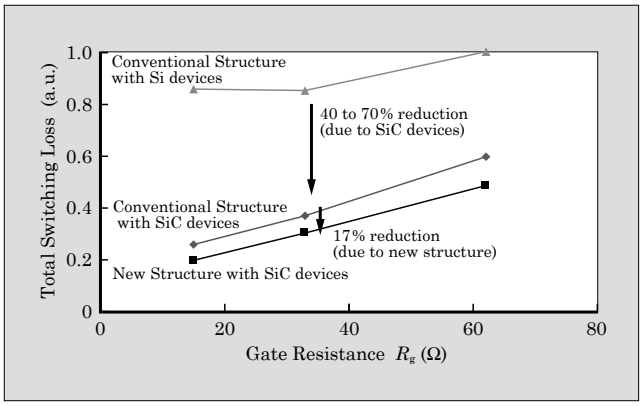

Fig.7 Loss evaluation by switching tests

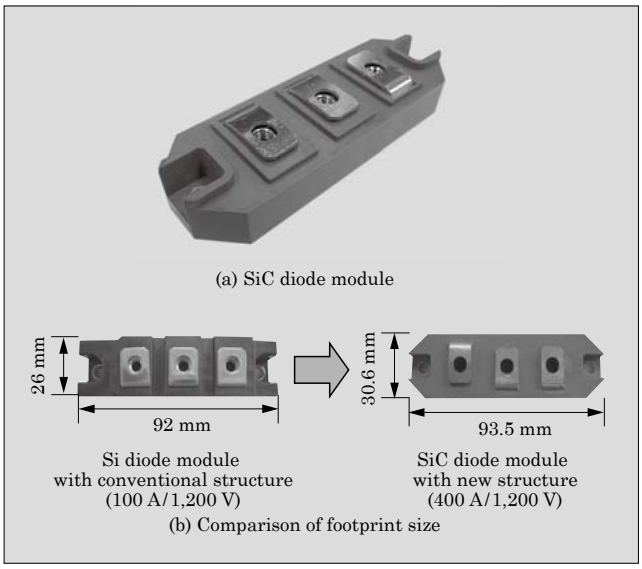

Fig.8 External view of SiC diode module and its footprint size

3.1 All-SiC module

The all-SiC module shown in Fig. 6(a) is 2-in-1 module rated at 100 A and 1200 V and equipped with SiC MOSFETs and SiC SBDs. The module has dimensions of 62.6 mm (length)×24.7 mm (width)×19.0 mm (height). Compared to a Si module having conventional structure and the same rating, the all-SiC module has a footprint of about half the size (see Fig. 6(b)).

The reasons for this small footprint size the all-SiC module are the new structure with Cu pin connection technology for the high-density mounting of power chips, the low thermal resistance structure for high thermal dissipation, and the low loss SiC devices and high temperature withstanding components having high reliability at high temperature operation.

Figure 7 shows the switching test results with different gate resistances of Si and SiC devices and different module structures in order to clarify the improvement in characteristics of the new structure and SiC devices.

The loss reduction with SiC devices is 40 to 70%, and a further 17% loss reduction is attributed to the new structure. The small parasitic inductance of the new structure as a result of the downsized current path is thought to limit the surge voltage and thereby reduce the switching loss.

3.2 SiC diode module

The SiC diode module shown in Fig. 8(a) is configured as a SiC SBD diode module with 2 arms in series and is rated at 400 A and 1200 V. The dimensions are 93.5 mm (length)×30.6 mm (width)×17.0 mm (height). Compared to a 100 A Si diode module with a conventional structure, this SiC diode module has four times the current density with about the same footprint size (see Fig. 8(b)).

4. Postscript

A new power module structure with Cu pin connections, Ag-sinter bonding and epoxy resin molding has been developed. This packaging technologies are able to take full advantage of the superior characteristics of SiC devices. Moreover, a prototype all-SiC module and SiC diode module were designed and their improved characteristics were evaluated.

In the future, Fuji Electric will verify the superior characteristics of this new power module through field tests and will continue to advance technology for the conservation of energy.

References

(1) Nishimura, Y. et al. Development of a Next-generation IGBT Module using a New Insulating Substrate. Fuji Electric Review. 2005, vol.51, no.2, p.52-56.
(2) Kobayashi, Y. et al. New Concept IGBT-PIM Using Advanced Technologies. Fuji Electric Review. 2007, vol.53, no.3, p.69-72.
(3) Morozumi, A. et al. Reliability Design Technology for Power Semiconductor Modules. Fuji Electric Review. 2001, vol.47, no.2, p.54-58.
(4) Horio, M. et al. “New Power Module Structure with Low Thermal Resistance and High Reliability for SiC Devices.” PCIM Europe. 2011, Proceeding CD, p.229-234.
(5) Ikeda, Y. et al. “Investigation on Wirebond-less Power Module Structure with High-Density Packaging and High Reliability, International Symposium on Power Semiconductor Devices and IC’s.” 2011, Proceeding CD, p.272-275.
(6) Horio, M. et al. “Ultra Compact, Low Thermal Resistance and High Reliability Module Structure with SiC Schottky Barrier Diodes.” IEEE Applied Power Electronics Conference and Exposition. 2011, Proceeding CD, p.1298-1300.

“Super J-MOS” Low Power Loss Superjunction MOSFETs

Takahiro Tamura † **Mutsumi Sawada** † **Takayuki Shimato** †

ABSTRACT

Fuji Electric has developed superjunction MOSFETs with an optimized surface design that delivers lower switching loss. In these “Super J-MOS”chips, gate length and channel density were adjusted to optimize the gate-to-drain capacitance and threshold voltage, thus achieving lower turn-off loss. For devices rated at 600 V/20 A/0.19 □, an extremely low turn-off loss of 160 μJ at the turn-off dV/dt of 10 kV/μs was realized. Power efficiency is over 94.0%, enabling compliance with the 80 PLUS certification.

1. Introduction

Recently, in response to heightened interest in global environmental protection through conserving energy and reducing CO_2 emissions, lower levels of power loss are sought in so-called IT equipment, such as PCs and servers. In order to reduce the power loss in IT equipment, the power conversion devices used in IT equipment must be made more efficient, and the technology that enables this higher efficiency is power semiconductors.

The power semiconductors installed in power conversion equipment operate as switching devices, and their power loss consists of conduction loss while the device is in its on-state, and switching loss when the device changes from its on- to off-state or from its off- to on-state. To achieve higher efficiency and lower loss in power conversion equipment, both types of loss must be reduced.

This paper reports on Fuji Electric’s successful development of a “Super J-MOS” (Superjunction MOSFET) that achieves low switching loss as a result of optimization of the SJ-MOSFET surface structures from a theoretical perspective and an improved trade-off relationship between turn-off loss E_{off}, generated when the device changes from its on- to off-state, and the value of turn-off dV/dt, which indicates the time-change of drain-to-source voltage at the time of turn-off.

2. Characteristics of the “Super J-MOS”

The use of an SJ-MOSFET is one way to reduce both conduction loss and switching loss. Compared to a conventional power MOSFET, the SJ-MOSFET features a significantly improved trade-off relationship between the device breakdown voltage BV_{DSS} and the specific on-resistance $R_{on}\cdot A$, and because the conduction loss can be reduced dramatically, SJ-MOSFETs are being used more and more in power conversion equipment.

Figure 1 shows schematic cross-sectional views of a SJ-MOSFET and a conventional MOSFET. The SJ-MOSFET has a structure in which p-pillars and n-pillars are arranged alternately in the drift region. By narrowing the width of each pillar, the impurity concentration in the drift region can be increased without decreasing the breakdown voltage, and therefore the on-resistance can be reduced.[(1)~(4)]

Furthermore, because an SJ-MOSFET has signifi-

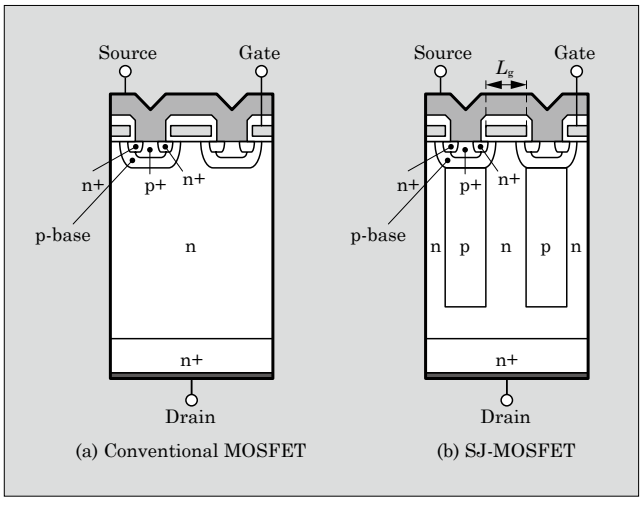

Fig.1 Schematic cross-sectional views of power MOSFETs

† Fuji Electric Co., Ltd.

*1: Miller period: See supplemental explanation 2 on page 88.

cantly smaller $R_{on} \cdot A$ than a conventional MOSFET, its gate-to-drain capacitance C_{GD} is also significantly smaller. As a result, there is a problem of the C_{GD} becoming too small, causing the gate controllability to decrease and the turn-off dV/dt to increase. Additionally, if the gate resistance R_g is increased in order to reduce the turn-off dV/dt, the Miller period*1 will lengthen and the loss will increase. As a result, the tradeoff relationship between E_{off} and turn-off dV/dt deteriorates. Accordingly, if the tradeoff relationship between E_{off} and turn-off dV/dt can be improved, and the turn-off loss decreased, a low power loss device that realizes both low conduction loss and low switching loss can be realized. In fact, the Super J-MOS is a realization of such a device.

3. Optimization of Surface Structures

3.1 Design concept

In order to improve the tradeoff relationship between E_{off} and turn-off dV/dt in a SJ-MOSFET, it is necessary to reduce turn-off dV/dt under conditions of constant R_g. Focusing on the reduction of turn-off dV/dt, characteristics of the tradeoff between E_{off} and turn-off dV/dt were improved in accordance with the following equation.

Assuming that the gate-source capacitance during turn-off is constant within the Miller period, turn-off dV/dt can be expressed as in Eq.(1).

$$\frac{dV}{dt} = \frac{\frac{I_D}{g_{fs}} + V_{th}}{C_{GD} \cdot V_{DS} \cdot R_g} \quad \cdots\cdots(1)$$

I_D : Drain current
g_{fs} : Transconductance
V_{DS}: Drain-to-source voltage

From Eq.(1), it can be understood that when R_g, I_D and V_{DS} are constant, increasing C_{GD} and decreasing the threshold voltage V_{th} are effective for reducing turn-off dV/dt. C_{GD} is determined by the distance between the p-bases, i.e., the gate length L_g, and therefore L_g should be lengthened in order to increase C_{GD}. Moreover, because V_{th} is determined according to the impurity concentration of the p-base region, V_{th} can be decreased by reducing the impurity concentration of the p-bases.

3.2 Gate length dependence of turn-off loss

Simulations based on the design concept were performed to estimate the L_g dependence of E_{off}. Figure 2 shows the L_g dependence of E_{off} and turn-off dV/dt. E_{off} values are shown for the case that turn-off dV/dt is 10 kV/μs, and turn-off dV/dt values are shown for the case that R_g is 91 Ω. Additionally, the values of L_g are relative to the value of L_g prior to optimization of the structure.

As shown in Fig. 2, turn-off dV/dt can be reduced by lengthening L_g, and the resulting decrease in the value of E_{off} was confirmed. When L_g increases above 1.4, the E_{off} value shows nearly no improvement and remains nearly unchanged. This is thought to be caused by the lengthening of the Miller period and increased loss that occurs when C_{GD} is increased, causing the turn-off time to become longer and the feedback capacitance to increase.

3.3 Threshold voltage dependence of turn-off loss

Next, the V_{th} dependence of E_{off} and turn-off dV/dt was calculated. The results are shown in Fig. 3. As in the calculation of the L_g dependence, the values of V_{th} are relative to the value of V_{th} prior to optimization of the structure. Additionally, an estimation of the V_{th} dependence was calculated based on the simulation described in Section 3.2 and using an optimal L_g design value of 1.4.

As shown in Fig. 3, turn-off dV/dt decreases as V_{th} becomes smaller, and accordingly, a decrease in the value of E_{off} was confirmed. If V_{th} becomes too small, however, a problem may occur in which the device turns-on unintentionally due to noise. In optimizing the design for V_{th}, it is necessary to be careful so as not to reduce V_{th} too much in order to prevent malfunction of the device.

Based on the above results and using L_g=1.4 and V_{th}=0.75 as optimal structure values, the tradeoff rela-

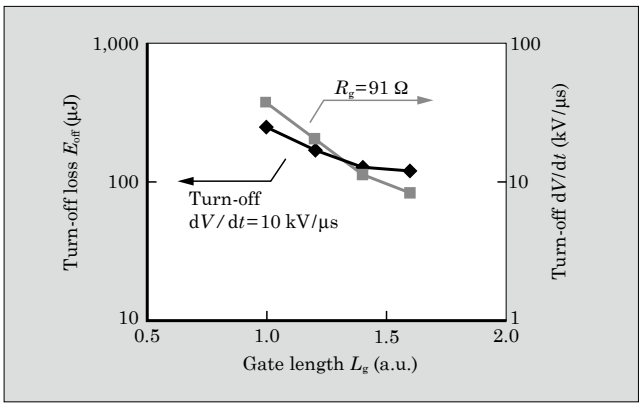

Fig.2 L_g dependence of E_{off} and turn-off dV/dt

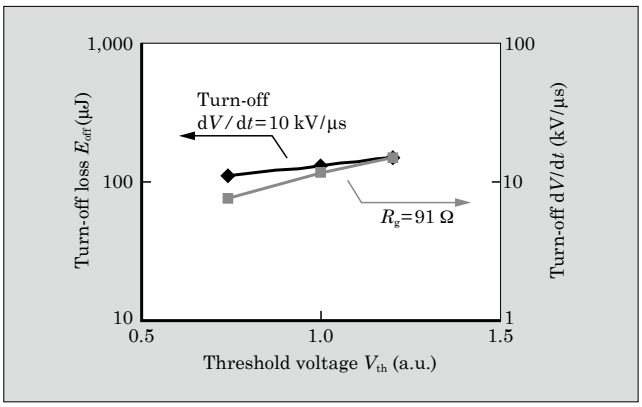

Fig.3 V_{th} dependence of E_{off} and turn-off dV/dt

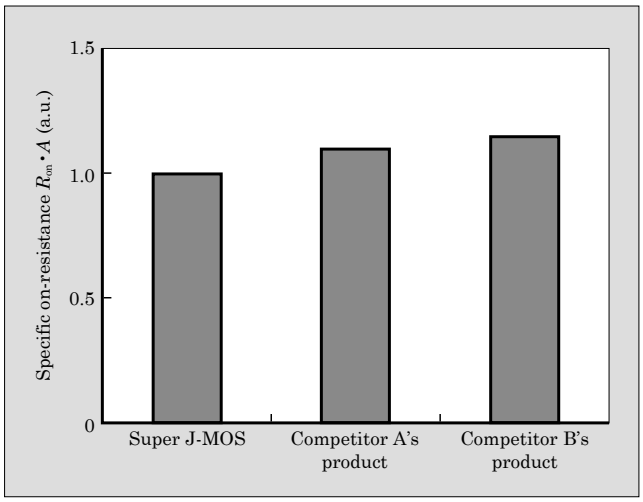

Fig.4 Comparison and evaluation of R_{on}・A

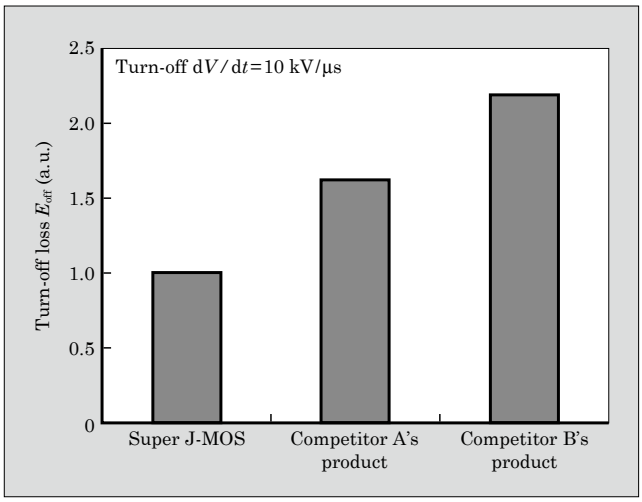

Fig.5 Comparison and evaluation of E_{off}

tionship between E_{off} and turn-off dV/dt was improved.

4. Super J-MOS Performance

4.1 Evaluation of on-resistance

For SJ-MOSFETs rated at 600 V/20 A/0.19 Ω, the specific on-resistances R_{on}・A at rated voltages of the Super J-MOS and competitors' products were compared and evaluated. Figure 4 shows the evaluation results. The values of R_{on}・A are relative to the value of the Super J-MOS. With the Super J-MOS, R_{on}・A values equal to or better than those of competitors' SJ-MOSFETs were confirmed.

4.2 Evaluation of switching loss

Next, E_{off} was evaluated. With the Super J-MOS, the E_{off} value is 160 μJ when turn-off dV/dt is 10 kV/μs, and this extremely small E_{off} was realized through structural optimization. E_{off} values when turn-off dV/dt is 10 kV/μs were compared and evaluated for the Super J-MOS and competitors' products, and the results are shown in Fig. 5. As in the case of Fig. 4, E_{off} values are relative to the value of the Super J-MOS.

As shown in Fig. 5, the Super J-MOS is affected by the structural optimization and the results showed an E_{off} value significantly lower than those of competitors' products.

5. Investigation in Electrical Equipment

As described above, by optimizing the surface structures, the Super J-MOS was confirmed to exhibit excellent levels of R_{on}・A and E_{off}. Next, to verify the power efficiency when using a Super J-MOS, a Super J-MOS was installed in the power factor correction (PFC) circuit of a 400 W-ATX power supply as shown in Fig. 6, and the power efficiency was evaluated. The same evaluation was also performed for company A's SJ-MOSFET, which exhibited lowest turn-off loss

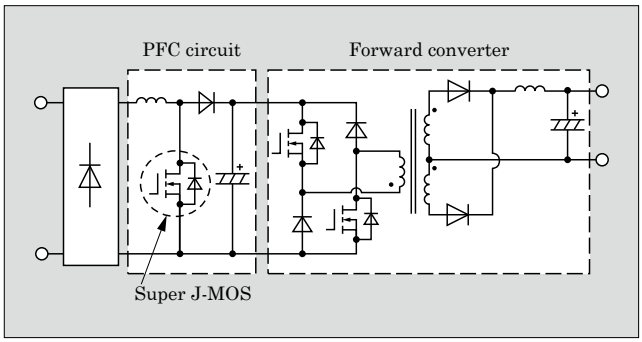

Fig.6 Configuration of PFC circuit

among the competitors' products. The values of power supply loss and power supply efficiency that were obtained were compared and evaluated (see Fig. 7). All the devices that were evaluated were rated at 600 V/0.19 Ω.

As shown in Fig. 7(a), in comparison to company A's product, the Super J-MOS exhibits lower loss especially during turn-off, and this contributes greatly to a reduction in total power supply loss.

Moreover, as shown in Fig. 7(b), highly efficient power supply operation is realized with the Super J-MOS, and when the power supply has a 50% load factor, the power efficiency is at the high level of 96%. Furthermore, in the load factor range from 20% to 100%, the power efficiency was at least 94% or higher. This result conforms to the "80 PLUS[6] "*2 standard, and indicates that the Super J-MOS possess characteristics that can contribute to improvement of the power

*2: "80 PLUS" : A standard promoting higher efficiency in power supplies and is defined by an independent private organization (http://www.80plus.org). In the power supplies used in PC and servers, 80 PLUS certification indicates that the power conversion efficiency is 80% or greater at load factors of 20%, 50% and 100%.
80 PLUS is a trademark or registered trademark of US-based Ecos Consulting Inc.

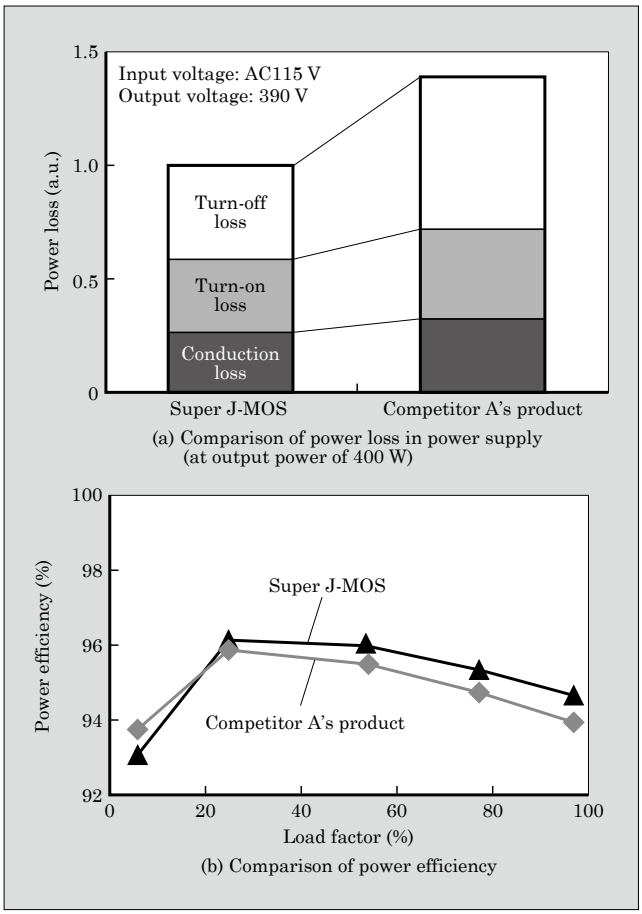

Fig.7 Results of investigation in electric equipment

efficiency of a power converter.

6. Postscript

By optimizing the surface structures of the SJ-MOSFET, the "Super J-MOS," which features an improved tradeoff relationship between turn-off loss and turn-off dV/dt and low switching loss, was developed. Increasing the gate-to-drain capacitance and lowering the threshold voltage was confirmed to result in a lower turn-off dV/dt and an improved tradeoff relationship between turn-off loss and turn-off dV/dt. By optimizing the surface structures of the device, the turn-off loss was found to be 160 μJ when turn-off dV/dt is 10 kV/μs, and this is an excellent level for a SJ-MOSFET. Additionally, as a result of installing a Super J-MOS in the PFC circuit of a 400 W-ATX power supply and then conducting an evaluation, power supply operation exhibiting much higher efficiency than that of competitors' SJ-MOSFETs was found to be possible.

Targeting applications in the communication and PC server power supply market, Fuji Electric is currently moving forward with efforts to reduce loss and increase the efficiency of the 600 V-rated Super J-MOS. Fuji Electric intends to continue to improve device performance in the future through device miniaturization and the like.

References

(1) Fujihira, T. "Theory of Semiconductor Superjunction Devices," Jpn. J. Appl. Phys., 1997, vol.36, p.6254-6262.
(2) Deboy, G. et al. "A New Generation of High Voltage MOSFETs Breaks the Limit Line of Silicon," Proc. IEDM, 1998, p.683-685.
(3) Onishi, Y. et al. "24 mΩcm² 680 V Silicon Superjunction MOSFET," Proc. ISPSD' 02, 2002, p.241-244.
(4) Saito, W. et al. "A 15.5 mΩcm²-680 V Superjunction MOSFET Reduced On-Resistance by Lateral Pitch Narrowing," Proc. ISPSD' 06, 2006, p.293-296.
(5) Baliga, B. J. Modern Power Devices, John Wiley & Sons, Inc., 1987, p.305-314.
(6) ECOS Consulting. http://www.80plus.org. (Refer to Jul. 29, 2011)

P-Channel Power MOSFETs for Space Applications

Masanori Inoue † **Akio Kitamura** † **Shuhei Tatemichi** †

ABSTRACT

Fuji Electric has added a family of p-channel power MOSFETs to its lineup of power MOSFETs for space applications. Depending on the application, designers can now choose between the existing n-channel power MOSFETs and the new chips, allowing them to reduce the system part count and achieve higher system reliability. Like the n-channel power MOSFETs, the new chips use quasi-plane junction technology to lower the resistance of the drift layer, thus lowering the on-resistance. A low-temperature process is used to form gate oxide films in all diffusion layers, achieving high total ionizing dose (TID) tolerance.

1. Introduction

That the benefits of utilizing outer space for such applications as communication satellites, meteorological satellites, GPS and earth observation have permeated our daily lives is well-known. The electronic devices and switching power supplies installed in artificial satellites are required to be highly efficient so as to efficiently utilize limited power in outer space and to have a reduced number of components so as to ensure system reliability. Moreover, the power metal-oxide-semiconductor field-effect-transistor (MOSFET), a key device for power conversion, is required to be a low loss device as well as to have high reliability against ionizing radiation[1] and to be resistant to high-energy charged particles (heavy particles)[2] and the like in a space environment.

Fuji Electric has previously developed and commercialized n-channel high-reliability power MOSFETs for space applications[3]. Recently, p-channel power MOSFETs for space applications have been newly added to Fuji Electric's product lineup. Compared to the n-channel power MOSFET, the p-channel power MOSFET has on-resistance that is 2 to 3 times larger in principle, and this is a disadvantage, but because its polarity is reversed, high-side switches and other circuits can be configured more simply. For this reason, the p-channel power MOSFET has the advantage of allowing the number of components to be decreased, thereby enhancing reliability and enabling a reduction in the size and weight of the overall system. Based on the technology cultivated with n-channel power MOSFET for space applications, Fuji Electric has developed and commercialized p-channel MOSFETs for space applications. The features and technology of these products are introduced below.

† Fuji Electric Co., Ltd.

2. Product Features

Table 1 lists Fuji Electric's product lineup of p-channel power MOSFETs, and Table 2 shows the differences in requirements for power MOSFETs for consumer-use and power MOSFETs for space applications. The MOSFETs for space applications maintain the equivalent low on-resistance of consumer power MOSFETs while providing the capability to tolerate a space environment.

2.1 Tolerance to ionizing radiation (TID tolerance)

Ionizing radiation is present in the environment along the orbit of an artificial satellite or the like. Generally, if a power MOSFET normally used at ground level is used in an environment of ionizing radiation, the breakdown voltage will decrease and the gate threshold voltage V_{th} that controls the on-off control of the power MOSFET will shift. The marketplace requirement for ionizing radiation tolerance is 1,000 Gy, which is the equivalent exposure as 10 years of geostationary orbit, and the ability to tolerate this level of exposure is ensured with the newly developed p-channel power MOSFET. Ionizing radiation tolerance is assessed by evaluating the change in characteristics that occurs when a product is actually irradiated with ionizing radiation. Figure 1 shows the evaluation results of breakdown voltage BV_{DSS} and V_{th}, which are particularly susceptible to ionizing radiation. BV_{DSS} does not change at all. Also, the shift in V_{th} is limited to within the range of the specification.

2.2 Heavy particle tolerance (SEE tolerance)

In space, heavy particles emitted from solar winds, supernova explosions and the like fly back and forth.

Table 1 Product list

Product type	V_{DSS} (V)	I_D (A)	I_D (Pulse) (A)	$R_{DS\ (on)}$ max. *1 (Ω)	P_D *2 (W)	V_{GS} (V)	$V_{GS\ (th)}$ (V)	Q_g max. (nC)	Radiation level (krad)	SEE *3 LET MeV/(mg/cm²)	Package type	Mass (g)
JAXA R 2SJ1 A0l	−100	−42	−168	0.045	250	±20	−2.5 to −4.5	230	100	37	TO-254	9.3
JAXA R 2SJ1 A02	−100	−25	−100	0.097	125	±20	−2.5 to −4.5	95	100	37	TO-254	9.3
JAXA R 2SJ1 A03	−100	−11	−44	0.226	62.5	±20	−2.5 to −4.5	40	100	37	TO-254	9.3
JAXA R 2SJ1 A04	−100	−42	−168	0.038	250	±20	−2.5 to −4.5	230	100	37	SMD-2	3.3
JAXA R 2SJ1 A05	−100	−29	−116	0.09	150	±20	−2.5 to −4.5	95	100	37	SMD-1	2.6
JAXA R 2SJ1 A06	−100	−13	−52	0.219	70	±20	−2.5 to −4.5	40	100	37	SMD-0.5	1.0
JAXA R 2SJ1 A07	−200	−35	−140	0.091	250	±20	−2.5 to −4.5	230	100	37	TO-254	9.3
JAXA R 2SJ1 A08	−200	−16	−64	0.21	125	±20	−2.5 to −4.5	95	100	37	TO-254	9.3
JAXA R 2SJ1 A09	−200	−7.5	−30	0.487	62.5	±20	−2.5 to −4.5	40	100	37	TO-254	9.3
JAXA R 2SJ1 A10	−200	−37	−148	0.084	250	±20	−2.5 to −4.5	230	100	37	SMD-2	3.3
JAXA R 2SJ1 A11	−200	−18	−72	0.203	150	±20	−2.5 to −4.5	95	100	37	SMD-1	2.6
JAXA R 2SJ1 A12	−200	−8.5	−34	0.48	70	±20	−2.5 to −4.5	40	100	37	SMD-0.5	1.0

*1 : $R_{DS\ (On)}$: V_{GS}=−12 V,
*2 : P_D: T_C=250°C
*3 : SEE: Kr, Energy: 520 MeV, Range: 63 μm, V_{DS}=rated V_{DS}, V_{GS}=+5 V

Table 2 Requirements of power MOSFET for space applications

Requirements		Consumer-use MOSFET	Space-use MOSFET
Ionizing radiation tolerance (TID tolerance)		×	◎
Heavy particle tolerance (SEE tolerance)		×	◎
Long-term reliability		○	◎
Electrical characteristics	Breakdown voltage	200 V	200 V
	On-resistance	◎	◎

TID : Total ionizing dose
SEE : Single event effect
◎: Fully meets requirements
○: Meets requirements
×: Does not meet requirements

The phenomenon in which a single incident heavy particle can cause degraded characteristics or permanent damage in a biased MOSFET is generically referred to as a "single event effect" (SEE). The probability of impact in space by a heavy particle with a larger mass is lower, but such a particle would have a large amount of energy and would have a significant effect on a MOSFET. The magnitude of the energy that a heavy particle would transfer to a MOSFET is described by the linear energy transfer (LET) of the particle. Additionally, the SEE tolerance also depends on the biased state of the power MOSFET at the time when the heavy particle comes in, and the higher the V_{DS} and V_{GS}, the greater the susceptibility to damage.

Therefore, the SEE tolerance is generally expressed with the magnitude of the LET and the useable areas of V_{DS} and V_{GS}. Figure 2 is shown for the power MOSFET at a LET value of 37 MeV/(mg/cm²). Because a reverse bias of +5 V or greater is not used with V_{GS}, in the actual useable area, the tolerance extends to the rated value of V_{DS}. The probability that a heavy particle having this LET value would collide with the MOSFET corresponds to approximately once every 200 years (estimated assuming an orbit altitude of 550 km and an orbital inclination angle of 31°), and

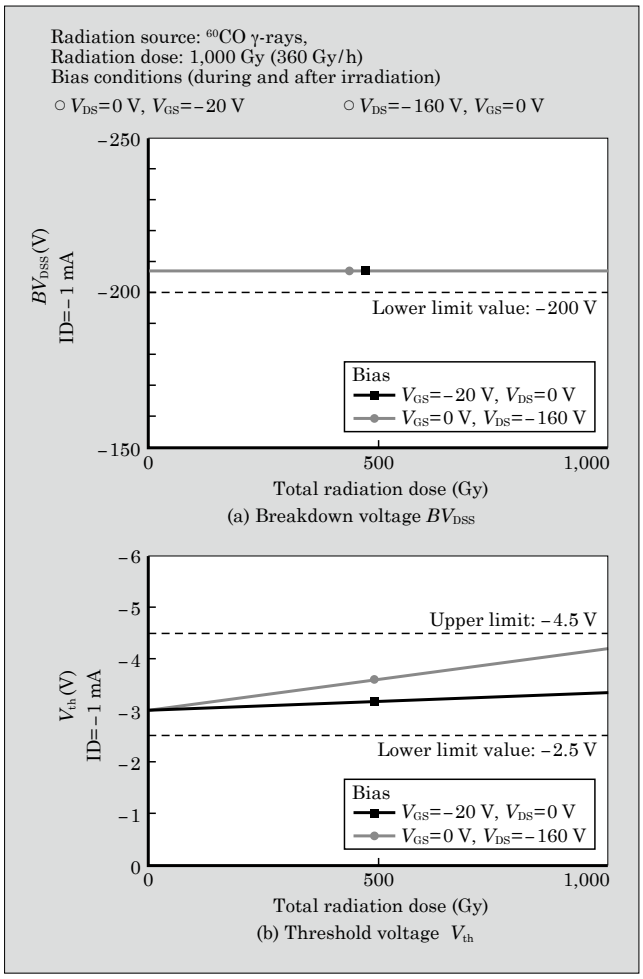

Fig.1 Tolerance to ionizing radiation (TID tolerance)

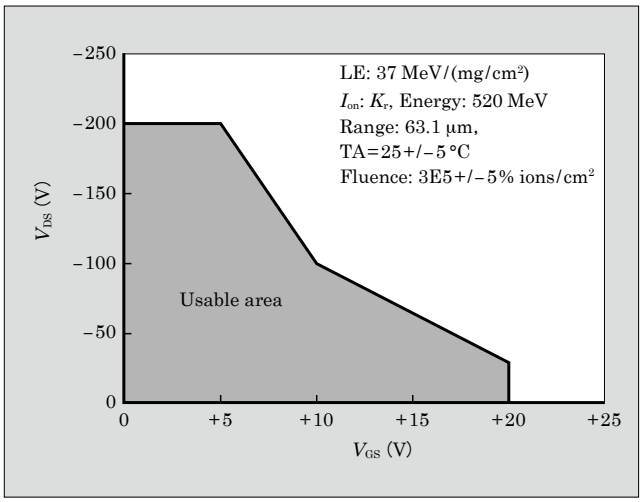

Fig.2 Tolerance to heavy particles (SEE tolerance)

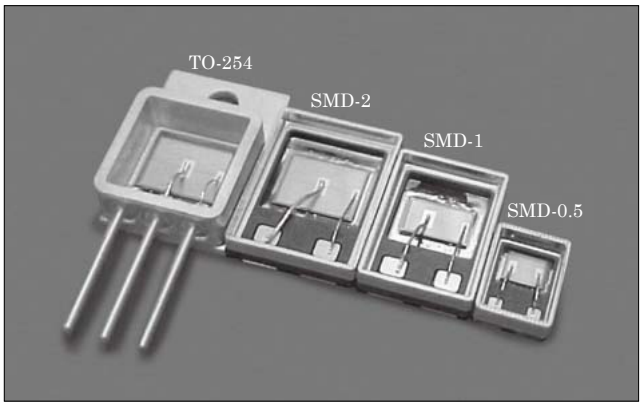

Fig.3 Internal structure of power MOSFETs for space applications

extremely high reliability against heavy particles is provided.

2.3 Long-term reliability

A metallic hermetically sealed package is used to ensure long-term reliability of the package. In order to improve thermal cycle tolerance, the package frame (part into which the MOSFET chip is mounted) is made from CuW (copper tungsten), which has a coefficient of thermal expansion extremely close to that of silicon (the material from which the MOSFET chip is made). Additionally, the hermetically sealed package is made hollow (Fig. 3) and filled with dry nitrogen to protect the power MOSFET chip from exogenous degradation modes.

3. Technology Applied to the MOSFETs for Space Applications

The technology developed for the previously commercialized 2nd generation n-channel power MOSFETs for space applications was also applied to these p-channel MOSFETs. This section introduces the technology for ensuring TID tolerance and low on-resistance.

3.1 Application of low-temperature process

The phenomenon of a V_{th} shift is caused by electrical charge becoming trapped in the oxide film as a result of ionizing radiation.

When a MOSFET is exposed to ionizing radiation, electrons and holes are induced in its oxide film. The holes, in particular, become trapped in the oxide film and form a fixed positive electrical charge that appears in the electrical characteristics as a shift in V_{th}.

From prior research, it is known that the greater the thermal history of exposure to high-temperatures, the greater amount of charge that will be trapped in an oxide film. In a consumer-use MOSFET, an efficient manufacturing process and stable electrical characteristics can be provided through the use of a gate electrode (on which a gate oxide film has also been formed) as a self-aligned mask. With this process, however, the gate oxide film acquires a thermal history of high-temperature exposure during the diffusion layer fabrication process, and the oxide layer ends up trapping a large amount of charge.

Therefore, a process flow in which the gate oxide film is formed after fabrication of the entire diffusion layer was applied to MOSFETs for space applications

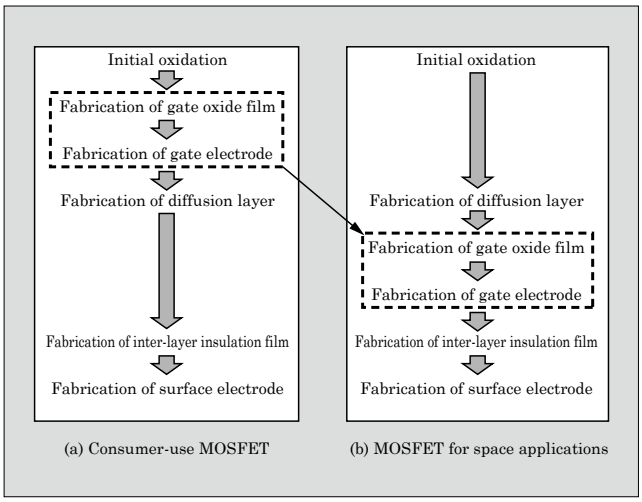

Fig.4 Process flow of consumer-use MOSFET and MOSFET for space applications

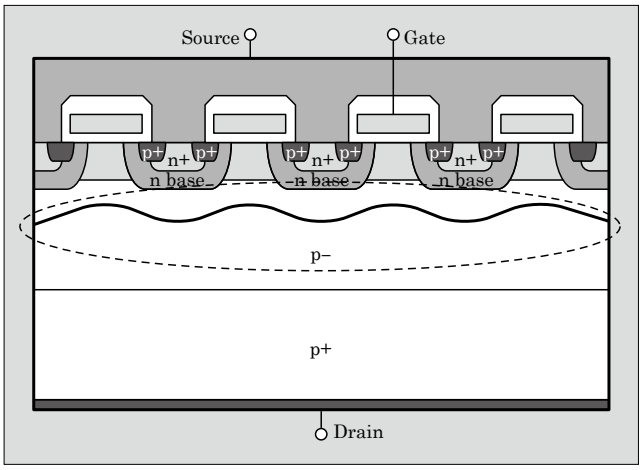

Fig.5 Cross-sectional view of active part of p-channel power MOSFET for space applications

(see Fig. 4). By applying this process, the gate oxide film acquired a lower temperature thermal history and a TID tolerance of 1,000 Gy was ensured.

3.2 Low on-resistance technology

The quasi-planer-junction (QPJ)[4] technology used in Fuji Electric's consumer-use MOSFETs was also applied to this MOSFET.

With QPJ technology, n-bases are arranged in a dense configuration and the interval between the n-bases is minimized to flatten the electric field and obtain a breakdown voltage close to that of a planar pn junction (see Fig. 5). As a result, this technology lowers the resistivity of the drift layer and reduces the on-resistance.

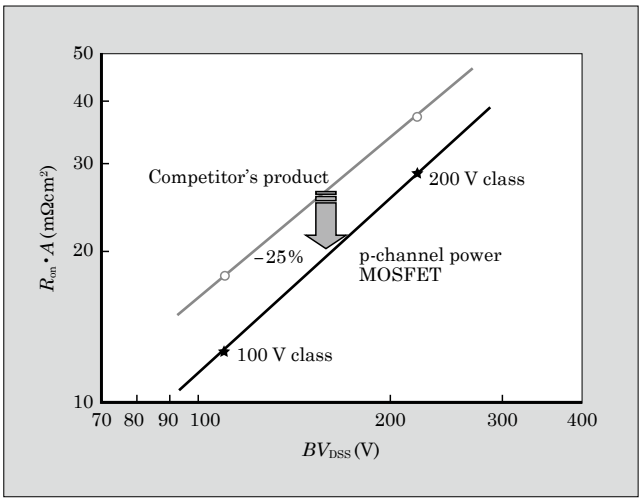

Fig.6 $R_{on} \cdot A$ versus BV_{DSS} tradeoff

The application of this QPJ technology resulted in a 25% reduction in on-resistance per unit area compared to that of a competitor's product (see Fig. 6).

4. Postscript

This paper has introduced Fuji Electric's p-channel power MOSFET for space applications. These MOSFETs are tolerant of the space environment, i.e., they exhibit good tolerance of ionizing radiation, heavy particles and so on, and also realize the low on-resistance of consumer-use power MOSFETs.

Fuji Electric will continue to endeavor to reduce on-resistance further, improve SEE tolerance, and to contribute to the promotion of space development in Japan and overseas.

References

(1) Gover, J. E. "Basic Radiation Effects in Electronics Technology." Colorado Springs, CO, Proc. 1984 IEEE NSREC Tutorial Short Course on Radiation Effects, July 22, 1984.
(2) Waskiewicz, A. E. et al. "Burnout of Power MOSFET with Heavy Ions of CaliFornium-252." IEEE Trans. Nucl. Sci. Dec. 1986, vol. NS-33, no.6, p.1710-1713.
(3) Inoue, M. et al. High Reliability Power MOSFETs for Space Applications. FUJI ELECTRIC REVIEW. 2010, vol.56, no.2, p.69-73.
(4) Yamada, T. et al. Power MOSFET 'Super FAP-G Series' for Low-Loss, High-Speed Switching. FUJI ELECTRIC REVIEW. 2001, vol.47, no2, p.41-44.

Supplemental Explanation

Supplemental explanation 1 3-level inverter technology

A multilevel-type inverter, as typified by a 3-level inverter, has many advantages over a typical 2-level inverter. As shown in the Figure, the voltage waveform at the conversion output part of the 2-level inverter is $\pm E_d$ pulse width modulated (PWM) pulses centered about the zero point, but in the case of a 3-level inverter, is combined PWM pulses of $\pm E_d/2$ and $\pm E_d$ centered about the zero point. Because the output waveform of the 3-level inverter more closely resembles a sine wave, the size of the LC filter used to convert the output waveform into a sine wave can be reduced. Furthermore, the switching loss occurring in a switch element is roughly halved and the noise generated by the equipment is also reduced, because the width of voltage fluctuation per one-time switch operation is half that of the 2-level inverter. The use of a 3-level inverter having these characteristics is effective for realizing smaller size and higher efficiency in a system.

For 3-level inverters, the method shown in the Figure in which an inverter is wired to the intermediate potential (N) of the DC power source, is known as the neutral-point-clamped (NPC) method. The naming of this method originates from the fact that the voltage applied to the switch element is always clamped to half the DC voltage E_d.

Compared to the NPC method, the advanced-NPC (A-NPC) method enables a simpler circuit configuration because the series-connected insulated gate bipolar transistors IGBTs have twice the rated voltage as the IGBTs used with the NPC method, and an reverse blocking IGBT is connected between the intermediate potential point (N) of the DC power source and an intermediate point (U) of the series-connected IGBTs. Having fewer current-conducting elements, the A-NPC method has the advantages of realizing lower loss and, when configuring the inverter, of requiring fewer number of power sources for the gate driving circuit.

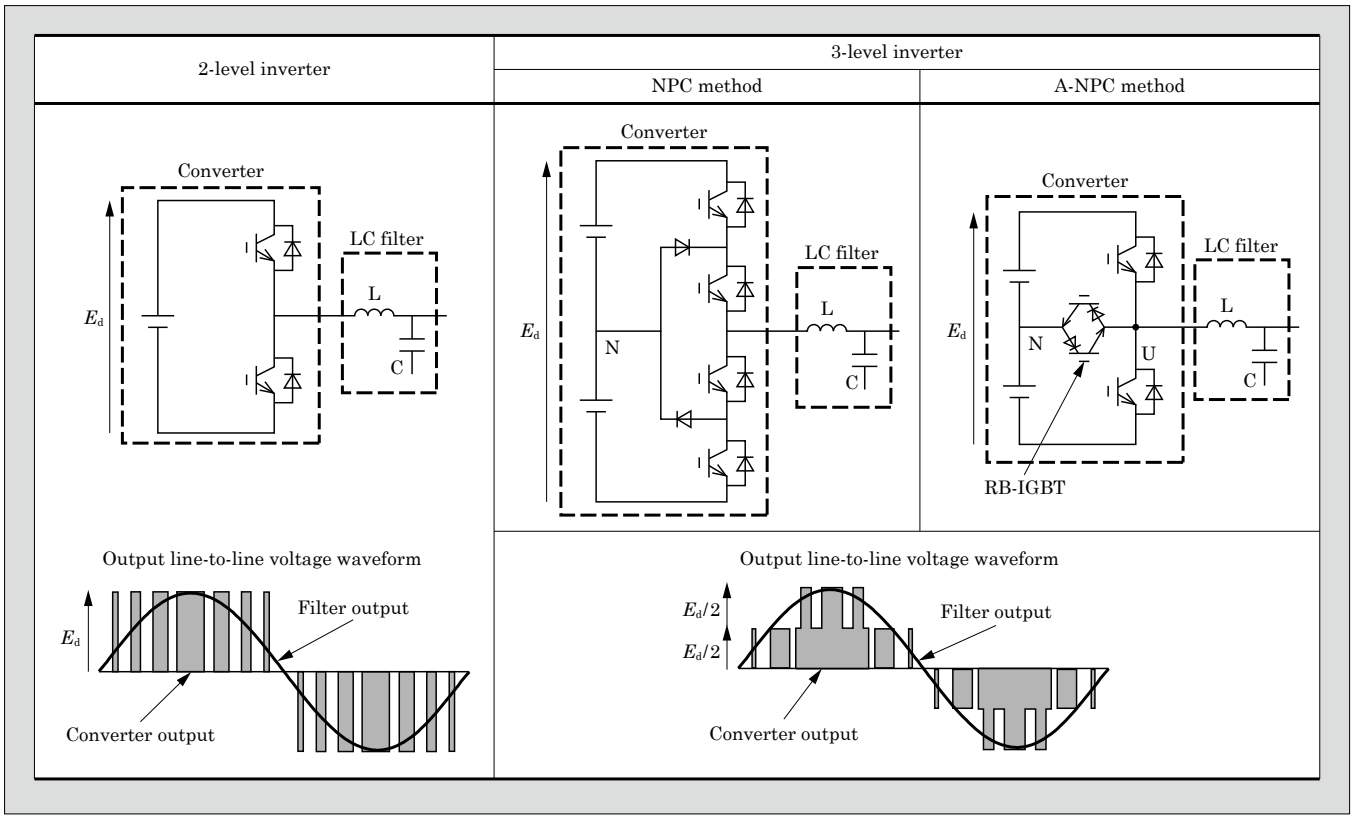

Figure Comparison of 2-level inverter and 3-level inverter circuits and voltage waveforms

Supplemental explanation 2 Miller period

In the switching of a semiconductor device, the gate capacitance is charged and discharged to turn-on and turn-off the device. At such times, changes in the drain-source voltage V_{DS} cause the gate-drain capacitance C_{GD} to change, and an interval occurs in which the gate-source voltage V_{GS} for charging and discharging C_{GD} becomes flat. This is known as the Miller period. The Figure shows a schematic of the L-load turn-off switching waveform of a power metal-oxide-semiconductor field-effect-transistor. As shown in Figure, when V_{GS} decreases, at the time t_0 when $V_{GS}=V_{DS}$, a depletion layer begins to expand on the gate to the drain and V_{DS} begins to increase. As a result, C_{GD} decreases and the Miller period is appeared. At the time t_1 when V_{DS} reaches the power source voltage, the depletion layer has stopped to expand, C_{GD} stops decreasing and the Miller period ends. At the end of the Miller period, V_{GS} and the drain current ID begin to decrease. The duration of the Miller period depends on the product C_{GD} and the gate resistance R_g, and therefore it is important that the device be designed such that loss does not increase with an extended Miller period.

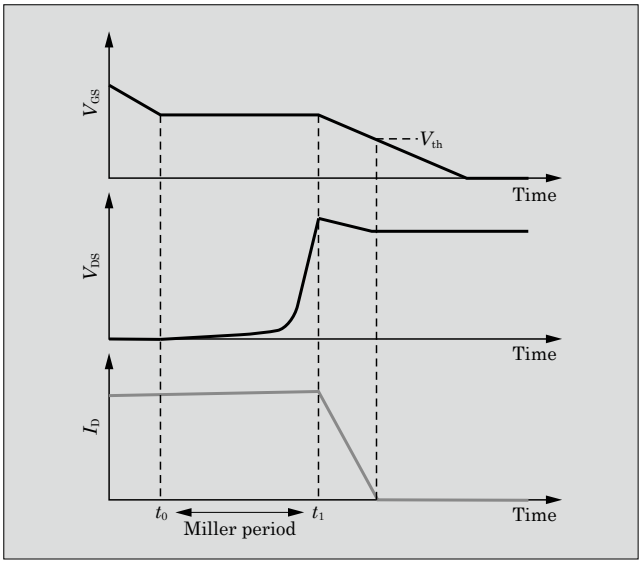

Figure Schematic diagram of L-load turn-off switching waveform

Overseas Subsidiaries

North America

Fuji Electric Corp. of America

Marketing, installation and repair of electrical machinery, control systems and electronic components

Tel +1-732-560-9410
URL http://www.fujielectric.com/fecoa/

EU

Fuji Electric Europe GmbH

Marketing, installation and repair of electrical machinery, control systems and electronic components

Tel +49-69-6690290
URL http://www.fujielectric.de/

Fuji Electric France S.A.S

Manufacture and sale of measuring and control devices

Tel +33-4-73-98-26-98
URL http://www.fujielectric.fr

East Asia

Fuji Electric FA (Asia) Co., Ltd.

Marketing of power distributors and control equipment

Tel +852-2311-8282

URL http://www.fea.hk/

Fuji Electric Dalian Co., Ltd.

Manufacture of low-voltage circuit breakers

Tel +86-411-8762-2000

Fuji Electric Taiwan Co., Ltd.

Semiconductor devices, power distribution and control equipment, sales of control, drive and rotating equipment

Tel +886-2-2515-1850

Fuji Electric (China) Co., Ltd.

Marketing of locally manufactured or imported products in China, and export of locally manufactured products

Tel +86-21-5496-1177
URL http://www.fujielectric.com.cn/

Fuji Electric (Shenzhen) Co., Ltd.

Manufacture and marketing of photoconductive drums

Tel +86-755-2734-2910
URL http://www.szfujielectric.com.cn/FUJIWebSite/index.html

Wuxi Fuji Electric FA Co., Ltd.

Manufacture and marketing of inverters in China

Tel +86-510-8815-2088

Fuji Electric Hong Kong Co., Limited

Sales of semiconductor devices and photoconductors

Tel +852-2664-8699
URL http://www.szfujielectric.com.cn/hkeng/company/index.htm

Shanghai Fuji Electric Switchgear Co., Ltd.

Manufacture and sales of switching equipment, monitoring and control appliances and related facilities

Tel +86-21-5718-1234
URL http://www.csfuji.com/

Fuji Electric Motor (Dalian) Co., Ltd.

Manufacture of motors

Hoei Hong Kong Co., Ltd.

Marketing, installation and repair of electrical machinery, control systems and electronic components

Tel +852-2369-8186
URL http://www.hoei.com.hk/eng/index.php

Fuji Electric (Changshu) Co., Ltd.

Manufacture and sales of electromagnetic contactors and thermal relays

Tel +86-512-5284-5642
URL http://www.csfe.com.cn/

Fuji Electric FA Korea Co., Ltd.

Sales of power receiving and distribution/control equipment and drive control equipment

Tel +82-2-780-5011
URL http://www.fujielectric.co.kr/

Shanghai Fuji Electric Transformer Co., Ltd.

Manufacture and sales of molded case transformers

Tel +86-21-5718-7705
URL http://www.csfuji.com/

Southeast and South Asia

Fuji Electric Asia Pacific Pte. Ltd.

Marketing, installation and repair of electrical machinery, control systems and electronic components

Tel +65-6533-0010
URL http://www.fujielectric.com.sg/

Fuji Electric Philippines, Inc.

Manufacture of semiconductor devices

Tel +63-2-844-6183

Fuji Electric (Malaysia) Sdn. Bhd.

Manufacture of magnetic disks

Tel +60-4-403-1111
URL http://www.fujielectric.com.my/

Fuji Electric Semiconductor (Malaysia) Sdn. Bhd.

Manufacture of semiconductor devices

Tel +60-4-494-5800

URL http://www.fujielectric.com.my/

Fuji Electric Power Supply (Thailand) Co., Ltd.

Manufacture and sale of small to mid-size UPS and internal electrical parts

Tel +66-0-2909-5998

Fuji Electric India Pvt.Ltd.

Sales of drive control equipments and semiconductor devices

Tel +91-22-4010 4870
URL http://www.fujielectric.co.in

Printed on recycled paper